Biomass Conversion and Biorefinery
https://doi.org/10.1007/s13399-023-04512-2

REVIEW ARTICLE

Biochar-based nanocomposites for industrial wastewater treatment via adsorption and photocatalytic degradation and the parameters affecting these processes

Enas Amdeha[1]

Received: 10 April 2023 / Revised: 12 June 2023 / Accepted: 15 June 2023

Abstract

The preparation of biochar (BC) as a useful substance generated from biomass valorization via pyrolysis has attracted much attention in recent years. Moreover, widespread worries about water pollution and the issues brought on by producing and releasing massive volumes of industrial effluents have sparked research initiatives to examine practical and affordable solutions to these problems. Dyes, heavy metals, and pharmaceutical compounds are the main hazardous pollutants in industrial wastewater. As a result, biochar (BC)/biochar (BC)-based nanocomposites have been presented as a potential alternative to handle wastewater pollution with both adsorption and photocatalytic degradation processes. Such nanocomposite materials benefit from the synergistic effect of adsorption and photocatalysis to attain improved removal of pollutants from industrial wastewater. Therefore, this review aims to describe different preparation methods for biochar and biochar-based nanocomposites. Furthermore, the differences between the adsorption and photocatalytic degradation processes are discussed. BC-based nanocomposites have emerged as promising adsorbents and photocatalysts for wastewater treatment applications. To maximize the efficiency of these processes, an overview of the parameters affecting pollutants removal from wastewater via adsorption and photocatalytic degradation processes is reviewed, where biochar dose, initial pollutant concentration, pH, temperature, time, the presence of different anions, and recycling are discovered to have a significant impact on their performance. Finally, future recommendations and research directions are provided to help shape the applications of BC-based nanocomposites for wastewater treatment applications. This review offers a comprehensive evaluation of the use of biochar as a new environmental material capable of removing pollutants from wastewater.

Keywords Adsorption · Biochar-based nanocomposites · Biomass valorization · Photocatalytic degradation · Pyrolysis · Wastewater treatment

Abbreviations

AO	Ammonium oxalate
BC	Biochar
BET	Brunauer–Emmett–Teller
BJH	Barrett-Joyner-Halenda
BPA	Bisphenol A
BQ	1,4-Benzoquinone
CB	Conduction band
CNT	Carbon nanotubes
CR	Congo red
CTAB	Cetyl trimethyl ammonium bromide
DMSO	Dimethyl sulfoxide
DRS	Diffuse reflectance spectroscopy
EDS	Energy-dispersive spectroscopy
EDTA	Ethylenediaminetetraacetate
FTIR	Fourier-transform infrared spectroscopy
HRTEM	High-resolution transmission electron microscopy
HTC	Hydrothermal carbonization
IPA	Iso propanol
MB	Methylene Blue
MBC	Magnetic biochar
MC	Mancozeb
MO	Methyl orange
NCs	Nanocomposites
NPs	Nanoparticles
OCPs	Organochlorine pesticides

✉ Enas Amdeha
enas_amdeha@yahoo.com

[1] Processes Design and Development Department, Egyptian Petroleum Research Institute (EPRI), 1 Ahmed El-Zomor St., Nasr City, Cairo, Egypt

Published online: 04 July 2023

pH_{PZC}	pH at point of zero charge
PL	Photoluminescence
RhB	Rhodamine B
ROS	Reactive oxygen species
Saf	Safranin O
SEM	Scanning electron microscope
SSA	Specific surface area
TA	Terephthalic acid
TEM	Transmission electron microscope
UV-Vis	UV-visible
VB	Valence band
XPS	X-ray photoelectron spectroscopy
XRD	X-ray diffraction
π-π EDA	π-π electron donor-acceptor

1 Introduction

The capacity of industrial manufacturing worldwide rose from 1.2 to 2.3 billion tons between 2000 and 2017, respectively, as a result of the fourth industrial revolution, increasing consequently the industrial effluents that discharge into water sources. These wastes are responsible for the death of about 1.6 million people in 2018, according to the World Health Organization (WHO) [1, 2]. Heavy metals, organic dyes, pesticides, phenols, wastewater pollutants from petroleum refineries, and some other typical industrial chemicals are examples of wastewater pollutants that are hazardous, refractory, and nonbiodegradable (persistent). For dyes for example, an estimated 15% of the world's total dye production is wasted during the dyeing process and discharged in the effluents from the fabric industry. By 2030, as compared to 2017, the number of chemical industries and hence their produced wastes/pollutants are anticipated to double. As a result, increasing public awareness of the dangers that synthetic chemicals pose to the environment and human health as well as improving waste management and pollution reduction are both necessary [3]. Moreover, by 2025, over one billion people will likely experience a water shortage, making the United Nations Sustainable Development Goal 6 (UN-SDG:6); calls for access to clean water and adequate sanitation; a top priority [4, 5].

As a result, solid waste-based materials have been introduced as a promising candidate to handle wastewater treatment, i.e., removing waste by waste to achieve dual goals (solid waste management and wastewater treatment in one process). The solid wastes produced by people's activities can be divided into three categories: industrial, agricultural, and municipal solid wastes [6]. The industrial waste can include hazardous materials and is created throughout the manufacturing, construction, and mining processes. Animal dung and crop remnants are examples of agricultural waste produced by farming operations. Food waste, paper, plastic, and other household products are all included in municipal waste, which is produced by homes, businesses, and institutions. According to some predictions, the world population will soon surpass 10 billion people, at which point there will be a significant increase in the requirement for food and other agricultural goods as well as the generation of agricultural solid waste. Worldwide, 7–9 billion tons of waste are produced annually [7, 8]. These wastes, including municipal, industrial, and hazardous wastes, have an impact on a variety of ecosystems, including soil (pH, texture, nutrient retention, and water holding capacity changes), water (pH, BOD, and COD that affect aquatic life), and air (decomposition of waste releases greenhouse gases), which in turn has an impact on human life and health in various ways. Recent reports have extensively discussed the thermochemical techniques that are used to produce biochar (BC) from these solid wastes. With different functional groups, wide surface area, high cation exchange capacity, high porosity, reusability, and stability, biochar is regarded as a practical and environmentally friendly substance [9–13].

Biochar can be produced from biomass via carbonization in the absence of oxygen (or in the presence of only a small amount). The main components of biochar are H, O, N, S, and C. The composition of the biochar and its features depend on the type of feedstock (lignocellulosic biomass), as well as the circumstances of preparation, such as temperature, biomass load, pressure, solvent, and catalyst. These key variables specify how much and what kind of biochar the thermochemical conversion processes produce. Pyrolysis, hydrothermal carbonization, gasification, and torrefaction are all considered forms of carbonization [14, 15]. According to operating circumstances such as temperature, residence time, heating rate, and pressure, these methods differ in terms of their respective co-products and maximum yields. Low carbonization temperatures (300–400 °C) lead to low porosity biochar. The most porous biochar is produced by carbonization at medium temperatures (400–700 °C), and it also has higher aromaticity, which encourages the interaction of electron donors. The oxygen and nitrogen surface groups could enhance functionality and serve as electron acceptors on the biochar surface at moderate pyrolysis temperatures [16–18].

Due to its stable structure, substantial specific surface area and pore volume, and abundance of active functional groups, biochar offers a wide range of application prospects in environmental remediation, particularly for wastewater treatment. Biochar is commonly used as an adsorbent material or catalyst in wastewater treatment for the removal of dyes, heavy metals, and other pollutants. It is essential to highlight that biochar's adsorption capacity is constrained, despite the fact that it may be manufactured from a range of easily accessible sources at a low cost. Due to their tiny surface areas and naturally negative surface charges, pristine

biochar often has a low capacity for adsorption, making it difficult to be used in highly concentrated effluent streams. Separating biochar from treated water is also challenging due to low density, tarry material leaching, and tiny particle size [19–21].

In order to get beyond biochar's limiting application, numerous experiments have been done to create innovative biochar-based nanocomposites by loading the biochar with a range of functional nanoparticles. These studies use biochar as the supporting material to anchor various nanomaterials. The novel composite materials have better physicochemical characteristics than pristine biochar, including more surface-active sites, a high specific surface area, higher porosity, stronger stability, and improved reusability. Different synthesis methods or altering the ratio and composition of the carbon matrix and nanomaterials can be used to create a range of composites. These innovative composites increase the potential to effectively adsorb and degrade various pollutants in wastewater by combining the superior catalytic characteristics of nanoparticles with the benefits of biochar's affordable price and reasonably high adsorption capacity [22, 23]. Furthermore, these composites provide a synergistic effect between the benefits of adsorptive biochar and the production of free radicals by the loaded nano-catalysts. Doping photocatalysts with non-metals (biochar) can improve the absorption of visible light, which has additional benefits. One of the most effective ways to remove various pollutants from wastewater and gaseous streams is adsorption. The contaminants are removed from the effluent during the adsorption process by being adsorbed on the active sites of the adsorbent. The fundamental mechanisms by which pollutants are efficiently adsorbed onto biochar are pore-filling, electrostatic interaction, creation of H—bonds, and π-π interaction between the biochar and the pollutants [24, 25].

Since wastewater pollutants are complex, advanced oxidation processes (AOPs), particularly photocatalytic degradation processes, are frequently used in wastewater treatment. Organic pollutants, nonbiodegradable chemicals, can be quickly degraded by AOPs into smaller or highly biodegradable fragments via the generation of some reactive oxygen species (ROS) mainly hydroxyl radicals ($^{\bullet}OH$) and superoxide ions ($^{\bullet}O_2$). Furthermore, because of its abundance of oxygen-containing functional groups, strong activation capability, and affordable production, biochar exhibits unique benefits as a catalyst in AOPs. In order to remediate pollutants through these processes, there has been an increase in interest in the study of the application of BC and BC-based nanocomposites for adsorption and combined usage with AOPs. This is an excellent chance to switch from a linear, single-component method to a multi-component one for wastewater treatment [26].

This review aims to summarize the synthesis methods of biochar and biochar-based nanocomposites from solid wastes, discussing the difference between these methods and their impact on the produced biochar. Also, to summarize the application of biochar-based nanocomposites in wastewater treatment via adsorption and photocatalytic degradation processes for the removal purposes of the present toxic pollutant. In addition, many factors that affect the mentioned wastewater treatment processes, e.g., biochar dose, pollutant concentration, pH, temperature, presence of anions, recycling etc., are discussed. The obstacles, as well as the future directions for BC-based nanocomposites for wastewater treatment applications, are mentioned.

2 Biochar

Biochar, which is distinguished by its rich carbon content, is produced by thermally processing biomass and agricultural wastes with little to no oxygen. It typically forms at temperatures between 400 and 700 °C. The varied biomass feedstock, the pyrolysis type, and the processed temperature, as well as its rate, are all factors that affect the physicochemical properties of biochar [27]. Publications regarding biochar and its applications in adsorption and photocatalytic degradation from 2017 up to 2021 have been growing rapidly (Fig. 1), which indicates that the application of biochar as promising adsorbents/ photocatalysts for wastewater treatment has gained the intensive interest of scientific researchers around the world.

2.1 Preparation of biochar

Thermochemical techniques such as pyrolysis, hydrothermal carbonization, and gasification have all been developed in order to obtain biochar (BC) from biomass in addition to bio-oil and non-condensable gases as byproducts. Pyrolysis, sometimes referred to as the devolatilization process, is the thermal breakdown of organic material by the application of heat at temperatures ranging from 250 to 900 °C in an oxygen-restricted or inert environment. One of the biggest benefits of this process is that it turns the feedstock into biochar, a substance rich in carbon that can produce synthetic gas and biofuel at higher temperatures or energies [28]. The cellulose, hemicellulose, and lignin in the feedstock undergo cross-linking, fragmentation, and depolymerization during decomposition to produce biochar, bio-oil, and syn-gas. The temperature, residence time, heating rate, and the utilized feedstock during the pyrolysis process all affect how much biochar is produced and characterized. The improvement of BC production conditions, particularly for agricultural and environmental usages, is a current effort to increase the quality of the prepared BC. Both fast and slow (traditional) conditions can be used for pyrolysis. Charcoal has been created by slow pyrolysis for countless years. The conversion of biomass into BC is typically referred to as slow pyrolysis

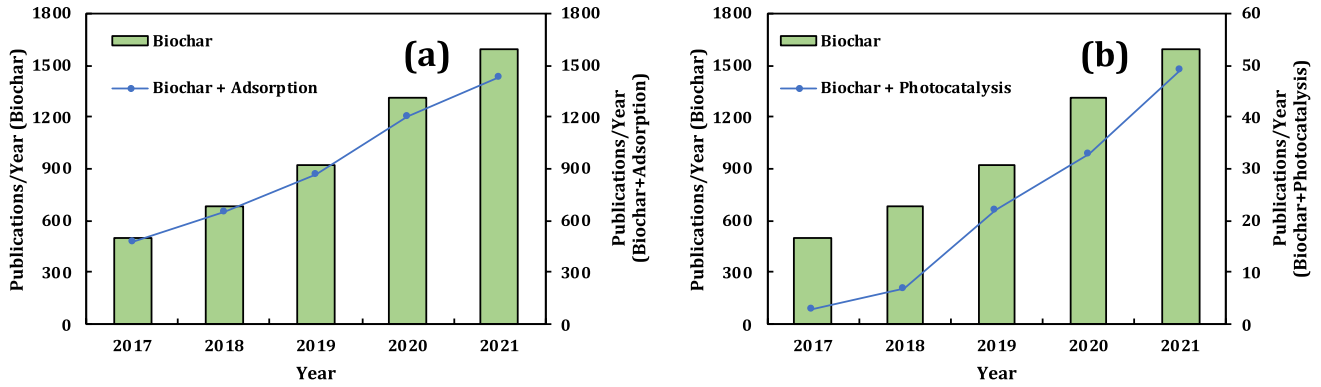

Fig. 1 Evolution of the number of publications on the application of biochar for adsorption (**a**) and for photocatalytic degradation (**b**) between 2017 and 2022 (data obtained from Scival on 6th July 2022, keywords used for the search were "biochar", "adsorption", and "photocatalysis")

when a long residence period (> two hours) is used. This method produces BC, bio-oil, and gas in nearly the same amounts regardless of the type of biomass used, and it uses a variety of reactor types to operate at atmospheric pressure. In general, a high BC yield is produced at slow pyrolysis conditions. Lignin and ash are present in large quantities in BC. Consequently, the particle size of produced BC is somewhat huge [29, 30].

Fast pyrolysis, on the other hand, is the process of heating biomass to reasonably high temperatures (500–1000 °C) over a brief period of time. When compared to slow pyrolysis, this method produces excessive quantities of bio-oil and non-condensable gases while producing comparatively little BC [31]. Biomass is typically pre-dried for quick pyrolysis (to less than 10 % water content) [32]. In general, plant tissues contain inorganics like S, P, and Cl as well as cations like K^+, Na^+, Ca^{2+}, Mg^{2+}, Fe^{3+}, and Al^{3+}. During the thermal processing of biomass, Al, Si, and P can hinder the biochar reactivity during their interactions with metals, resulting in the creation of aluminates, silicates, and phosphates, respectively. By raising the pyrolysis temperature (to around 700 °C), heteroatoms are eliminated, and the reactions can cause the formation of the graphene layer. Additionally, sulfur is released from the char content at temperatures below 500 °C degrees due to protein degradation. However, some of these elements combine with metallic elements like K and Ca to generate K_2S and CaS, respectively, and this portion is what remains in the biochar [33]. At low temperatures, large molecules, such as heteroatoms, can prohibit the graphene-like layers from closing, which leads to the creation of micropores. Alkaline earth metals, on the other hand, inhibit the synthesis of such molecules, which reduces the porosity of the biochar.

The hydrothermal carbonization process (HTC) is regarded as a practical method for producing biochar since it can be carried out at low temperatures between 180 and 250 °C. In order to set hydrothermal carbonization apart from other manufacturing methods, the name "hydrochar" is given to the final product. The feedstock and water are combined in this procedure, and the reactor is then sealed. In order to preserve stability, the temperature is raised gradually. Hydrolysis, dehydration, decarboxylation (which releases CO_2), and aromatization are just a few of the processes that happen throughout the process. Since HTC does not require drying of the used biomass before the process, it can create biochar or hydrochar with a higher carbon content than other processes because most biomass contains moisture and needs to be dried separately. By lowering the hydrogen to carbon (H/C) and oxygen to carbon (O/C) ratios, this process, which occurs at high temperatures and pressures, produces hydrochar that is rich in carbon [11, 34].

Torrefaction is a thermal process for producing high-quality solid biofuels in an oxygen-restricted environment under atmospheric pressure. It is a developing method for the manufacture of biochar. In fixed bed reactors, the torrefaction process occurs. The end result is a stable, homogeneous, high-grade biofuel with greater energy and calorific value than the input feedstock. This allows for considerable logistical, handling, and storage advantages as well as a wide range of applications. When the temperature is between 200 and 300 °C, the residence duration is shorter than 30 min, the heating rate is less than 50 °C/min, and there is no oxygen present, torrefaction, a type of incomplete pyrolysis, takes place. The wastes from forestry and agriculture are more suitable for the torrefaction process, in which cellulose decomposition occurs above 280 °C and hemicellulose decomposition occurs at 240 °C [35].

Another thermochemical process called gasification converts organic material into small amounts of CO, CO_2, H_2 gas, and methane (CH_4). Gasification takes place at high temperatures between 700 and 800 °C in a regulated oxygen environment. The majority of the products are gases, with BC coming in second place (around 10%) and liquid products coming in last (in very small amounts) [28]. According to Fig. 2, the type of process, synthesis circumstances, and

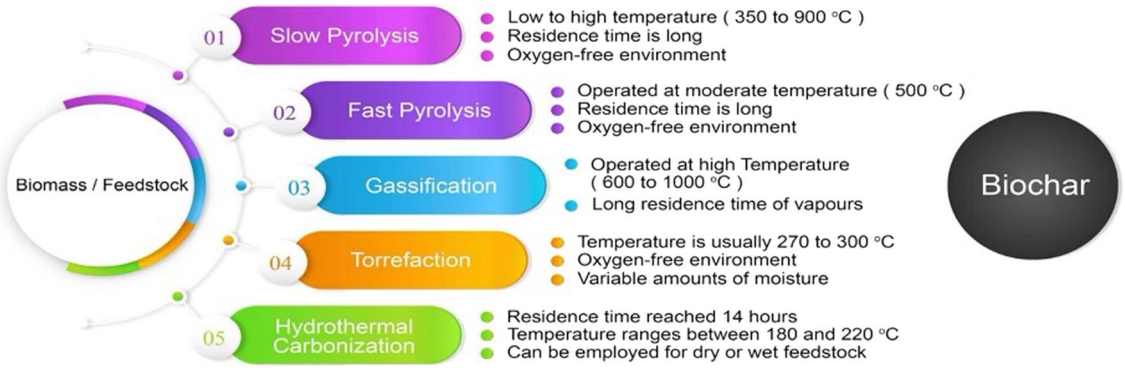

Fig. 2 Sustainable concept of biochar production with different techniques [36]

feedstock material are mostly responsible for the characteristics and effectiveness of the biochar that is formed [36].

The pyrolysis temperature had an effect on the BC samples morphology. For this regard, Vieira et al. [30], studied the morphology of BC obtained from rice husk (RH) at different pyrolysis temperatures 300, 400, and 500 °C. It is possible to notice the morphological differences between RH and BC samples, and between BC samples obtained at different temperatures, Fig. 3. SEM of RH (Fig. 3a) shows peaks and globular forms distributed along a dense surface, without the existence of apparent superficial faults. If compared to RH, Fig. 3b shows that the surface of BC obtained at 300 °C presented smaller peaks and more dispersed and irregular globular forms. Moreover, there were holes on the surfaces, which are possibly due to the removal of volatile matter and lignocellulosic content. The proximate analysis showed that there is a large amount of volatile matter in this BC sample. For the BC sample at 400 °C (Fig. 3c), there are no original peaks on the surface and there are not as many globular structures as before, but an increase in size and quantity of holes. For this BC sample, the proximate analysis indicated significant amounts of unextracted volatile matter, but in smaller quantities than in samples collected at 300 °C. Thus, pyrolysis at 400 °C has also been interrupted before a complete devolatilization of the biomass sample. For the BC sample at 500 °C (Fig. 3d), the original structures became non-existent, and a new morphology can be seen as channels along the entire surface. Possibly, these visible structures are mostly attributed to lignin [37]. The proximate analysis of these BC samples showed average volatile matter content of 4.56%, thus indicating that the pyrolysis process was more effective than other BC collected at lower temperatures. Other authors presented similar results [37–39].

Table 1 lists some of the detected effects of pyrolysis temperature on BC characteristics. The conversion of solid waste to BC frequently fulfils the sustainability criteria. For example, a wastewater treatment facility produces sewage sludge, an organic waste with high levels of nitrogen, phosphorus, and micronutrients that requires an effective management approach to prevent further environmental problems [40].

2.2 Biochar-based nanocomposites

Biochar-based nanocomposites with the best features of both materials could be prepared by nanomaterial engineering. The limitations of employing pristine biochar when trying to remove contaminants from an aqueous solution are solved through the synthesis of biochar-based nanocomposites. The following two techniques are primarily used to prepare biochar-based nanocomposites: (1) integrating nano-metal or their hydroxide; (2) pretreating biomass or post-treating the pyrolyzed biochar with the metal salt [49, 50]. The properties of biochar nanocomposite can be improved by merging the benefits of nanomaterials with the presence of several functional groups in pyrolyzed biochar, for example —OH, —COOH, and amino acids. These functional groups are crucial to the use of biochar, particularly when it comes to the removal of different pollutants from wastewater. Additionally, the nanocomposites are more effective due to their intrinsic large specific surface area, which results from the properties of both the nanomaterial and the biochar. Researchers have looked into adding nanoparticles to biochar, and they discovered that it improved its physicochemical characteristics. The research made it possible to address the problems associated with using pristine biochar for wastewater treatment by overcoming its basic limits [51]. Although some of the nanoparticles contained in the matrix could leak into treated water if not securely anchored, interests have been raised concerning the stability of these biochar-based nanocomposites after being used. The usage of magnetic biochar nanocomposites has been investigated to address these issues. With the extra benefit of recycling the nanocomposites after being used, this method might make it simple to separate the magnetic nanocomposite, even with

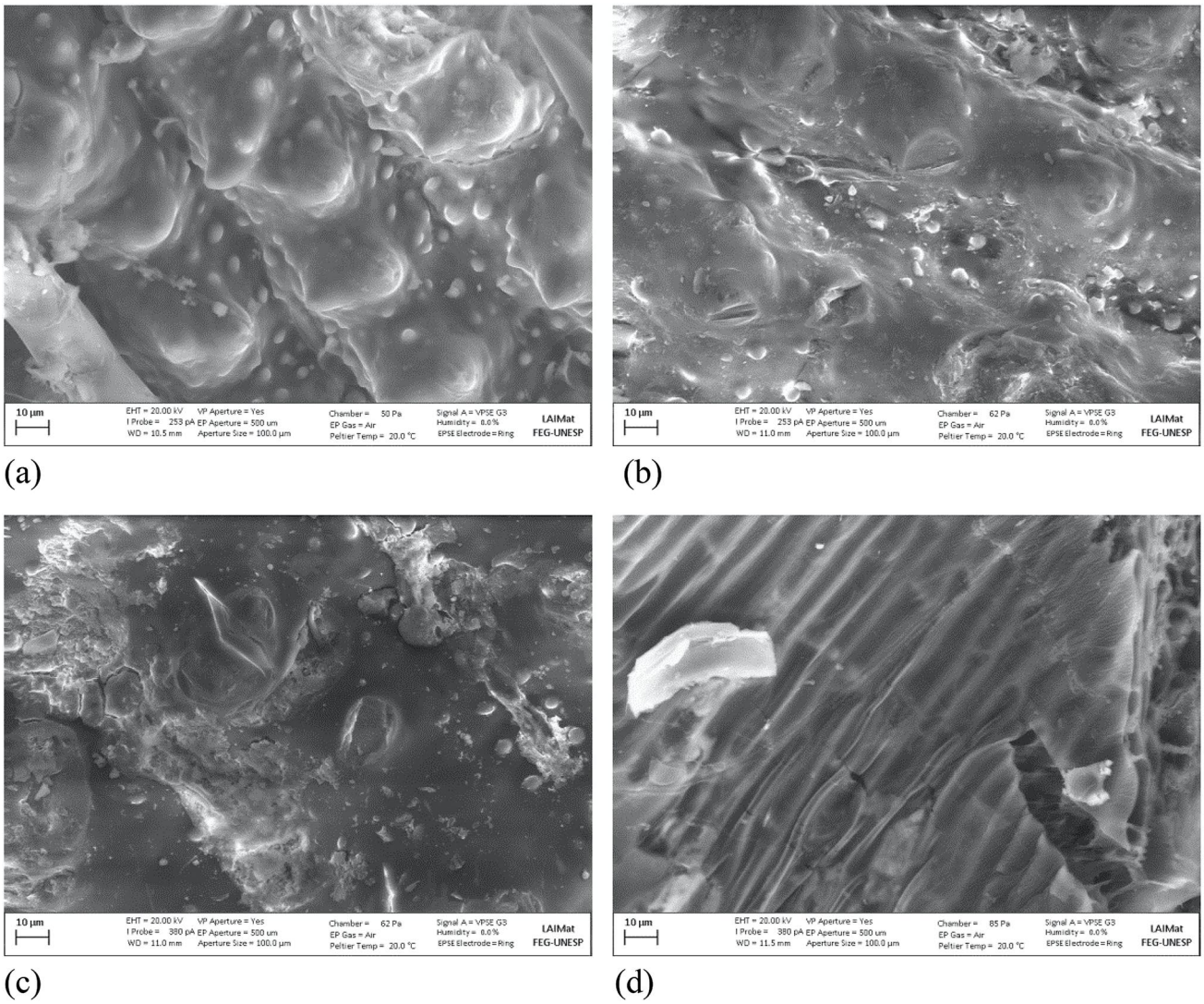

Fig. 3 SEM images (magnification x 1500) of husk rice (**a**) and samples of rice husk biochar obtained at 300 °C (**b**), 400 °C (**c**), and 500 °C (**d**) [30]

a regular magnet. According to research, the magnetite/biochar nanocomposite prepared by pre-treating biomass with $FeCl_3$ composites had exceptional ferromagnetism capabilities that allowed the composite to adsorb pollutants containing arsenic [52]. Moreover, there have been reports of carbon nanotubes (CNT) being incorporated into BC. CNT-BC composites were able to possess a high surface area (359 m^2/g) and a greater pollutant adsorption effectiveness due to the high surface area of BC and the CNTs. Similar outcomes were shown when graphene was pre-treated with wheat straw biomass waste using a slow pyrolysis process, and the graphene coating on the surface of the BC upgraded the surface properties. In contrast to the limited adsorption characteristics displayed by the pristine biochar, additional functional groups were added, and excellent adsorption of phenanthrene and mercury pollutants was observed [53].

2.3 Preparation of biochar-based nanocomposites

The sol-gel, hydrothermal, mechanical mixing, and sonication treatment processes are the most frequently used techniques for preparing biochar-based nanocomposites. The best-recorded performances of biochar-based nanocomposites have also been achieved by the mechanical mixing technique. For example, *Salvinia molesta*-based biochar has been impregnated with TiO_2 using mechanical mixing. The resulting composite performed superior to one made using

Table 1 Effects of BC production temperature on its properties

BC type	Condition	Main properties	Ref.
White-wood BC	High temperature	No acidic functional groups as they are lost under high temperature.	[41]
Corn-stover, red-oak BC	Moderate temperature (500 °C) High temperature (700 °C)	High CEC, but low AEC, PZSE and PZNC[a] Low CEC and high AEC, PZSE and PZNC[a]	[42]
Coppiced wood-lands BC	High temperature crop residue and manure BC	High ash content	[43]
Sugarcane bagasse BC	Pyrolysis at (300–600 °C)	By increasing the used temperature, the BC's average pore diameter is decreased.	[28]
Cow manure-loaded BC	Low temperature	There are volatile organic compounds (VOCs).	[44]
Pitch pine BC	Pyrolysis (300–500 °C)	By increasing the used temperature, the BC yield is decreased from 60.7% to 14.4%	[45]
Miscanthus BC	Temperature > 360 °C	High thermal and biological resistance to degradation	[46]
Hardwood oak-based wood pellets	Pyrolysis (400–600 °C)	Increasing the used temperature, converting the labile C forms to aromatic C structures in BC	[47]
Boiled radix isatidis residue BC	Pyrolysis (300–700 °C)	Increasing temperature results in a reduction of VOCs, strengthens the carbon enrichment	[48]

[a]) *CEC*, cation exchange capacity; *AEC*, anion exchange capacity; *PZSE*, point of zero salt effect; *PZNC*, point of zero net charge

the sol-gel approach. The ratio of BC and TiO_2 precursor materials may have a more significant impact on the composite's photocatalytic performance than the impregnation process [54]. Innovative, practical, sustainable, and uncomplicated approaches must be used for the synthesis routes. As a result, depending on the precursor materials and the method employed to produce the composite, the properties of nanocomposites differ significantly. The surface areas of the BC-TiO_2 nanocomposites are typically lower than those of pristine BC but substantially higher than those of TiO_2. For example, under identical experimental circumstances, the surface areas of TiO_2, BC-TiO_2, and BC were 0.39, 102, and 1058 m^2/g, respectively [55]. Due to the nanoparticles' adhesion to BC's active areas, the surface area of BC is decreasing. In addition, mesoporous surface structures of BC are more practical for TiO_2 composition than microporous ones in order to prevent the risk of pore structure blocking. Meanwhile, the adsorbents' cationic or anionic surface functional groups encourage chemical interactions, particularly their ability to remove ions through ion exchange [56]. The illustration of the BC-TiO_2 production process as a model for BC-based nanocomposites using the sol-gel, ultrasonic, and hydrothermal techniques is shown in Fig. 4. The hydrothermal method is a widespread solution-based reaction technique that operates in a wider temperature range, from ambient temperature to moderately high temperatures. This approach has the benefit of morphological control based on high or low temperatures. Additionally, this technology

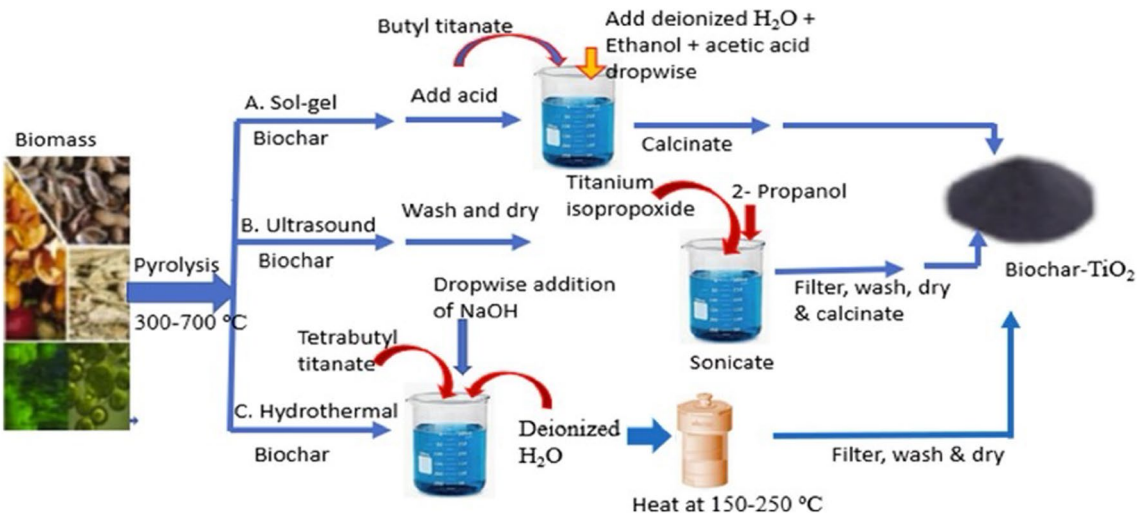

Fig. 4 The preparation of BC-TiO_2 nanocomposites using different methods [26]

makes it simple to control the composition, size, and forms of a variety of high-quality crystalline nanomaterials. The main drawbacks of this approach are that it requires pricey autoclave equipment and that the chemical reaction occurs at a temperature and pressure that are relatively high. The sol-gel technique (a wet chemical process) can prepare a range of high-quality BC-based nanomaterials. The benefits of this process include the ability to operate at a range of temperatures, the fabrication of homogeneous and pure nanomaterials, and the simplicity with which complicated nanostructures and composites can be fabricated. Nevertheless, the drawbacks include a prolonged processing time and a high precursor cost [57]. Due to its easy-to-use, eco-friendly, and quick nature, as well as its ability to produce smaller-sized nanomaterials and a variety of different nanostructures, ultrasonic techniques have seen significant growth recently. The sonochemical reduction rate is governed by the ultrasonic frequency being used.

3 Wastewater treatment applications

For treatment of various wastewater pollutants, many processes have been established such as precipitation, ion-exchange processes, sedimentation, biological treatments, adsorption, and photodegradation using heterogeneous photocatalysts, etc. Among these mentioned techniques, the adsorption and the photocatalytic degradation stands out as promising processes due to their advantageous as mentioned below [58–60].

3.1 Adsorption process

One of the most significant processes for the removal of various environmental contaminants is adsorption, which is regarded as a sustainable, scalable, practical solution to combat environmental pollution. Adsorption is a flexible process because of its distinct qualities, including energy concerns, cost-effectiveness, and simplicity. By means of physical or chemical forces, pollutants can move from the liquid phase to a solid phase in a process known as adsorption. Several adsorption mechanisms, including H—bonding, electrostatic, π–π interactions, and mixtures of these interactions, are required for the removal of hazardous pollutants. Due to its efficiency, economy, and environmental friendliness, the adsorption method has been widely employed in industrial wastewater treatment and soil remediation [61, 62]. Generally, researchers have given adsorption a lot of thought, and a number of materials have been prepared to help with the adsorption of pollutants from wastewater. Because they have specific adsorption properties on different pollutants, conventional adsorbents such as activated alumina and resin are widely used. To address the challenge that there are poor adsorption performances for some pollutants, finding novel forms of adsorbents with high performance, cheap cost, recyclability, and simple application is highly recommended. As a suitable loading matrix, biochar and nanocomposites based on it are currently one of the most important research topics [63].

3.2 Photocatalytic degradation process

Photocatalysis has been presented as one of the most effective methods for degrading organic pollutants. This is due to its being straightforward, has a high-efficiency rate, eliminate harmful organic compounds without spreading pollutants from one phase to another, reproducible, safe for the environment, and simple to handle [64–66]. Photocatalyst is the backbone of the photocatalysis process that is responsible for the process performance. As an alternative to pristine BC and photocatalysts, BC-based nanocomposites have been developed. BC serves as an electron acceptor in nanocomposites and significantly improves photodegradation performance. Particularly extensive applications in catalytic degradation can be found for photocatalytic BC-based nanocomposites. The preparation of these nanocomposites using metallic oxides and waste products can improve both the management of environmental wastes and the removal of contaminants. The surface area and active sites of BC nanocomposites are increased while stability and dispersion are improved [19, 67]. One advantage of BC nanocomposites that contain photocatalytic nanoparticles is a reduction in the energy band gap. Because of their light sensitivity, non-toxicity to the environment, chemical stability, abundance, and low cost, semiconductor materials like TiO_2 nanoparticles make effective photocatalysts. The broadband gap and quick electron-hole pair recombination are a problem for this semiconductor. Although it is currently expensive and impractical to dope transition metals, combining them with BC in hybrid systems is a potential way to close such gaps. Metal doping has benefits like narrowing the band gap and enhancing the absorption of visible light, but it also has drawbacks like low thermal stability of composites, generation of secondary pollution, and photo-corrosion, and an increase in the rate of recombination of electron-hole pairs when present in excess [68]. Before applying the nanocomposite on a pilot or industrial scale, it is crucial to stabilize it to lessen its adverse effects. The synergetic photocatalytic degradation of pollutants is now the preferred method over BC adsorption. This hybrid process provides a preferred way to deal with the complicated and varied types of polluted wastewater. With their diverse surface chemistry, BC nanocomposites have strong interaction capabilities to deal with a variety of pollutants that are present in different concentrations at the same time.

The photocatalysis process is based on the reaction between pollutants and strong oxidizing and reducing agents (h^+ and e^-) produced by UV or visible light irradiation on photocatalyst surfaces. When exposed to light (UV, visible, or solar light), photocatalytic processes primarily use semiconductor catalysts like CuO, SnO_2, TiO_2, Fe_2O_3, Fe_3O_4, and ZnO to degrade pollutants. When exposed to light, the photocatalyst is activated, causing photogenerated electrons to move from the valence band (VB) to the conduction band (CB), creating electron/hole pairs (e^-/h^+) [69, 70]. After the production of the electron-hole pair, the reduction at the surface of the photocatalyst is occurred by the photogenerated electron (e^-) and oxidation at the surface of the photocatalyst by the photogenerated hole (h^+). When the donor molecule is oxidized by the h^+ in the VB, reactive oxygen species (ROS), including hydroxyl radicals ($^\bullet OH$), are created. The hydroxyl radical ($^\bullet OH$) is produced when the donor molecule reacts with the water molecules. Superoxide ions ($^\bullet O_2$) are created by the reaction of oxygen species in the solution with e^- from the CB. The oxidizing and reducing agents, h^+ and e^-, are both effective. The oxidation and mineralization of pollutants by the h^+ in the VB leads to the production of CO_2 and water as the byproducts of the reaction [71, 72]. In order to oxidize pollutants made of organic chemicals, the h^+ can also react with water to produce $^\bullet OH$. The below equations (Eq. (1)–Eq. (12)) and Fig. 5 provide a general overview of potential reactions that could take place during photocatalysis. Sometimes, a recombination between positive holes and negative electrons can occur (Eq. (2)), causing a release of energy in the form of excitons, by measuring these excitons by photoluminescence technique (PL), the recombination rate can be measured. Whenever, the low the recombination rate the high the photocatalytic activity.

$$\text{Excitation}: \text{Photocatalyst} + h\nu \rightarrow e^-_{CB} + h^+_{VB} \quad (1)$$

$$\text{Recombination}: h^+ + e^- \rightarrow \text{energy} \quad (2)$$

$$\text{Oxidation}: h^+ + H_2O \rightarrow \bullet OH + H^+ \quad (3)$$

$$h^+ + OH^- \rightarrow \bullet OH \quad (4)$$

$$h^+ + \text{organic pollutant} \rightarrow \text{oxidized pollutant} \quad (5)$$

$$\text{Reduction of adsorbed } O_2: e^- + O_2 \rightarrow \bullet O_2^- \quad (6)$$

$$\text{Reaction with } H^+: \bullet O_2^- + H^+ \rightarrow \bullet OOH \quad (7)$$

$$2 \bullet OOH \rightarrow O_2 + H_2O_2 \quad (8)$$

$$H_2O_2 + \bullet O_2^- \rightarrow \bullet OH + OH^- + O_2 \quad (9)$$

$$H_2O_2 + h\nu \rightarrow 2 \bullet OH \quad (10)$$

$$\text{pollutant} + \bullet OH \rightarrow \text{intermediates} \quad (11)$$

$$\text{intermediates} \rightarrow CO_2 + H_2O \quad (12)$$

In Eq. (6), oxygen is depicted as preventing electron recombination and promoting the generation of peroxide ($O_2^{\bullet -}$) free radicals. The hydroperoxide radicals ($HO_2^\bullet$) that are created from those radicals can then be protonated once again to create hydrogen peroxide, an extremely potent oxidizing agent [3].

3.3 Comparison between adsorption and photocatalytic processes

The removal of various chemical pollutants from wastewater using the adsorption and photocatalytic degradation processes is quick and effective. In addition to addressing the drawback of adsorption, which is the transfer of pollutants from one phase to another resulting in the production of secondary waste by the end of the adsorption process, photocatalytic degradation is an environmentally friendly process because the photocatalysts are benign to the environment as this process eliminates the major concern of the used adsorbents' disposal [74]. The chemical pollutant is either totally

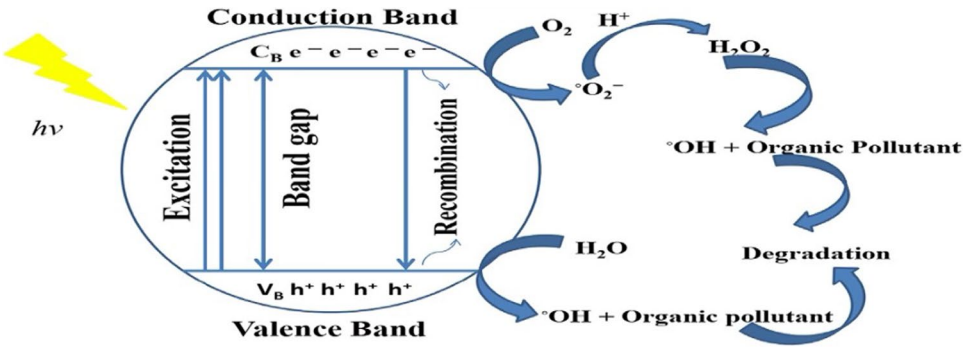

Fig. 5 General photocatalytic degradation mechanism [73]

mineralized by the photocatalytic degradation process to produce CO_2 and H_2O as the end products or converted into less hazardous or toxic byproducts. By completely removing the pollutant, the photocatalytic degradation process has proven to be more effective than adsorption. The materials used in wastewater treatment must have the ability to be stable and recyclable for sustainable engineering. Desorption has been recognized as a technique for regeneration in adsorption systems. It is crucial to choose an eluent that will not harm the adsorbent material and is both economical and environmentally benign [75]. Acid eluents had the highest desorption efficiency for regeneration, according to Vakili et al. [76], who included desorption agents like salts, alkalis, acids, and chelating acids.

Chemical, thermal, and biological processes are also available for regenerating the used adsorbents. The efficiency of the adsorbent can be decreased by reusing the adsorbents multiple times because some of the pollutant molecules that were not desorbed into the solution can leak out, but this is not a problem with photocatalyst because the pollutant has already been degraded [77]. It is interesting to note that in the majority of photocatalytic degradation processes, adsorption is crucial because pollutants are first adsorbed on the surface of the photocatalyst, where they are then exposed to light through the active species or hole. Since the surface area of the photocatalyst is crucial for the charge transfer, a lot of researchers have found that the adsorption accelerates photodegradation. Materials having potential for adsorptive and photocatalytic activity have been created in some research. Wei et al. [78] further demonstrated that adsorption improved the photocatalytic degradation of MB using CeO_2/g-C_3N_4 and that photodegradation led to the regeneration of the adsorption sites on the photocatalyst. A further comparison between these two processes is shown in Table 2.

4 Biochar-based nanocomposites as adsorbents

Biochar has attracted a lot of attention recently for its use in the removal of harmful pollutants from wastewater streams.

4.1 Adsorption of inorganic pollutants

When Khan et al. [84] employed biochar prepared from Japanese oak wood for their adsorption investigations on the arsenite As(III) and arsenate As(V), it was found that the pristine biochar exhibited reasonably performance for the removal process. In which, As(V) was more easily absorbed than As(III) (84 and 8%, respectively). The capacity of biochar has been expanded through modifications to deal with various pollutants. The source of biochar, its modifications, and the experimental settings are all related to the performance of removing different pollutants. Khan et al. [85] prepared perilla leaves-derived-BC at different temperatures; 300 °C and 700 °C, and found that the BC prepared at 700 °C was more successful than the BC prepared at 300 °C, particularly for the removal of As(III) compared to As(V). They came to a conclusion that when competed to BC synthesized at 300 °C; BC prepared at 700 °C had a larger specific surface area favoring the adsorption of As. The most effective methods for increasing the ability for environmental pollutants to be adsorbed have also been shown to be alkali treatment and impregnation with nanomaterials.

Ahmed et al. [86] successfully prepared biochar from rice straw (BR) and subsequently fabricated hydroxyapatite (HAP) biochar nanocomposite (BR/HAP) through a co-precipitation method to be used as a new and efficient adsorbent for removing U(VI) from aqueous solution. Characterization of both raw biochar and the nanocomposite via BET, SEM,

Table 2 Concise comparison between adsorption and photocatalytic degradation processes

Basis/factors	Adsorption	Photocatalysis	Ref.
Cost	Economical.	Expensive (light sources, reactors and some of the semiconductors are costly).	[73]
Efficiency/Safety	Efficient but has the defect of secondary waste generation.	Highly efficient and ecofriendly.	[79]
Ease of application	Easy to operate and adaptable.	Not too easy to operate when it comes to using a photoreactor (requires expertise).	[80]
Duration	Takes time (some reactions can last for days for optimum performance).	Very fast.	[69]
Process conditions	Affected by operational parameters like adsorbent dose, pH, contaminant concentration, ionic strength, temperature, etc.	Affected by the same operational parameters like adsorption process in addition to light intensity, and dissolved oxygen species.	[81]
Recycling	Some adsorbents are not recyclable due to irreversible pore deformation.	Can be recycled mostly.	[82]
Pollutants	A wide range of contaminants from organic, inorganic and microbial can be treated.	Outstandingly for organic pollutants.	[83]

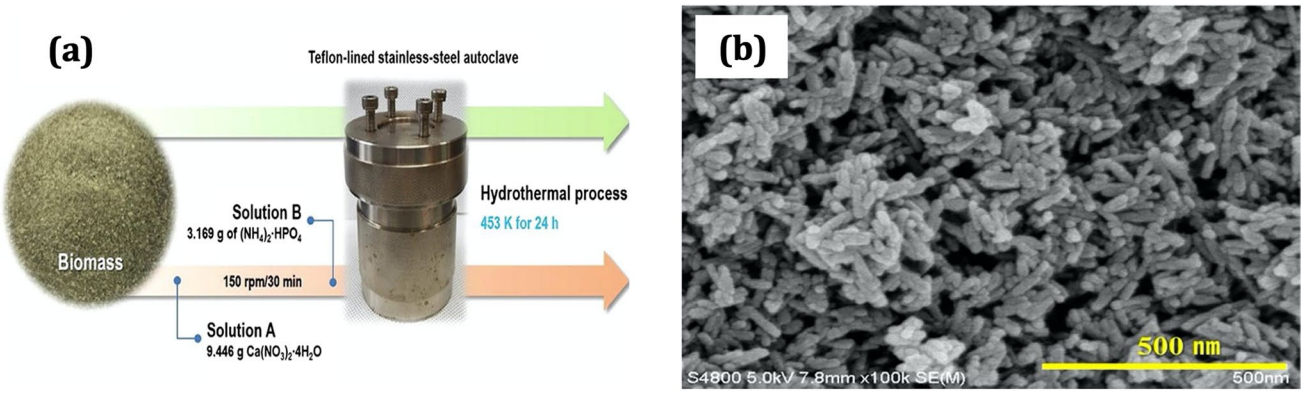

Fig. 6 (**a**) Hydrothermal synthesis of HAP/BC-NCs; (**b**) SEM image of the HAP/BC-NCs [87]

EDS, TEM, XRD, FTIR, and XPS techniques confirmed that BR/ HAP was successfully prepared. The results of the batch tests revealed that, in comparison to BR, the obtained BR/HAP had a superior ability for U(VI) removal with a higher adsorption rate which is less than 30 min. For BR and BR/HAP, the maximum adsorption capacities were, respectively, 101 mg/g and 423 mg/g. A pseudo-second-order kinetic model that completely explained the adsorption kinetics gave the maximum U(VI) adsorption capacities (q_e) for BR and BR/HAP of 110 mg/g ($R^2 = 0.98$) and 428 mg/g ($R^2 = 0.99$), respectively. This would imply that chemical adsorption via diffusion or surface complexation would control the adsorption of U(VI) by the BR/HAP composite as a single-layer process. The Langmuir isotherm model ($R^2 = 0.97–0.99$) was fitted to the experimental data in order to accurately simulate the adsorption of U(VI) onto BR and BR/HAP. The thermodynamic data showed positive values for ΔH° and ΔS°, indicating the endothermic nature of U(VI) adsorption onto both adsorbents and an increase in molecular randomness, and negative values for ΔG°, unequivocally establishing the reaction was spontaneous. The fundamental mechanisms were ion exchange with UO_2^{2+} and surface complexion by –OH and –COOH. Additionally, even after five adsorption-desorption studies, the BR/adsorption HAP's capacity still stands at >90%, demonstrating good reusability and stability. Because of this, BR/HAP may be a strong candidate to be employed as an adsorbent for the removal and recovery of U(VI) ions from wastewater.

In order to prepare hydroxyapatite/biochar nanocomposites (HAP/BC-NCs) for the adsorption of copper (Cu(II)) from aqueous media, Jung et al. [87] synthesized *Undaria pinnatifida* roots-derived-biochar (BC) by a hydrothermal method (Fig. 6a). The produced HAP/BC-NCs' surfaces successfully incorporated rod-shaped HAP nanoparticles, as shown by the results of the characterization (Fig. 6b). Batch experiments demonstrated that two potential pathways for the removal of Cu(II) from aqueous solution, cation exchange between Cu^{2+} in solution and Ca^{2+} in the HAP, and the formation of inner-sphere surface complexes on the surfaces of the HAP/BC-NCs, are possible. The adsorption procedure adheres to a pseudo-second-order model, as shown by kinetic model. A higher effectiveness for Cu(II) adsorption than previously reported composite materials was determined to be 99 mg/g at 25 °C, which is the maximum adsorption capacity. A Langmuir isotherm model well represented adsorption isotherms. The thermodynamic analysis revealed that the process was spontaneously endothermic and thermodynamic.

Since magnetic BC has shown to be more effective than non-magnetic BC for removing different types of pollutants, the preparation of magnetic BC composites has attracted a lot of attention in recent years. According to Yi et al. [88], the effectiveness of BC against environmental pollutants can be significantly increased by using magnetic BC materials. According to Tan et al. [89], adding magnetic compartments (Fe^{2+}/ Fe^{3+}) to rice straw prior to pyrolysis caused the production of hematite (γ-Fe_2O_3) while keeping the original functional groups of biochar (–OH, –COOH, C=O, C=C, and C–O–C), which improved cadmium adsorption. The formation of γ-Fe_2O_3 during pyrolysis can also aid in the adsorption of heavy metals. Because oxygen-containing functional groups like CO_3^{2-} and PO_4^{3-} are formed under CO_2 pyrolysis conditions, the scientists claimed that BCs synthesized under these conditions have increased adsorption capacities for heavy metals. This behavior may be attributed to the presence of CO_2 that possess an excellent affinity to react with hydrogenated and oxygenated groups resulting in increasing the specific surface area and hence the adsorption performance [90].

Bai et al. [91] prepared bagasse biochar/ferrite (BB/FE) nanocomposite via microwave pyrolysis method, using sugarcane bagasse waste as raw material for the adsorption of As(V) from wastewater. Under the experimental conditions, the maximum As(V) adsorption capacity of 12.8 mg/g was

successfully achieved. The synergistic effect of bagasse biochar and ferrites on As(V) adsorption was comprehensively investigated by TEM, FTIR, XPS, adsorption thermodynamics and kinetics analysis, and DFT calculations. The findings indicated that electrostatic attraction played a major role in the As(V) adsorption process. The iron arsenate floccules that were produced as a result of the reaction between the adsorbed arsenates and ferrites on the nanocomposite were entirely eliminated by magnetic separation after they had formed on the material. In addition, to create a new method for using bagasse wastes, this work offers theoretical recommendations for the preparation of high-performance nanocomposite adsorbents.

4.2 Adsorption of organic pollutants

For the first time, Yao et al. [92] developed BW(Ni) magnetic *wakame* biochar nanocomposites for the adsorption of methylene blue (MB) dye. Magnetic biochar samples were prepared using the impregnation procedure, which involves loading nickel onto wakame charcoal through a single carbonization stage at 800 °C while using different concentrations of KOH as an activation agent. The highest MB adsorption capacity (479 mg/g) of the BW(Ni)0.5 at 20 °C was observed under adsorption equilibrium. The pseudo-second-order model was more consistent with the kinetic data, and the Langmuir isotherm equation was a better fit for the adsorption behavior. The adsorption reaction also included an endothermic, spontaneous mechanism. The magnetically activated biochar nanocomposite still has a high adsorption capacity (117 mg/g) for MB after five cycles, according to the recycling studies utilizing magnetic separation. This work suggests that large-scale industrial wastewater treatment in the future can be anticipated to the usage of BW(Ni)0.5 to MB's strong adsorption performance.

Prajapati and Mondal [93] fabricated Fe_3O_4-onion peel biochar nanocomposites (Fe_3O_4-OPBC NCs) for the adsorption of Cr(VI), Congo red (CR) and Methylene blue (MB) dyes. These NCs were prepared using an environmentally friendly process that involved low-temperature pyrolysis in two inert atmospheres of N_2 and CO_2 gas. Surface functionality, surface area, and pollutant removal capacity of the synthesized NCs were all impacted by the change in the inert gaseous atmosphere in the pyrolysis reactor. The O/C ratios for Fe_3O_4-OPBC-(N_2) and Fe_3O_4-OPBC-(CO_2) were found to be 2.05 and 1.89, respectively. This shows that the CO_2-treated atmosphere was more advantageous for the higher surface area and porosity but the content of active functional groups was reduced. The inert N_2 atmosphere was more advantageous for the higher content of oxygen and nitrogen-containing functional groups in the NCs but resulted in less porosity and less surface area in the NCs. At pH 2 in the solid adsorbent, Cr(VI) was reduced by Fe_3O_4-OPBC-(N_2) and Fe_3O_4-OPBC-(CO_2) NCs, producing more than 64 and 48% Cr(III), respectively. The quick reduction rate demonstrated by Fe_3O_4-OPBC-(N_2) NCs was brought on by the oxygenated functional and polycyclic aromatic groups, which are good at transferring electrons. According to these results on the uptake of Cr(VI), CR, and MB dyes, the Fe_3O_4-OPBC-NCs' heterogeneous surface was a favorable environment for Freundlich multilayer chemisorption. Fe_3O_4-OPBC-(N_2) had a maximum adsorption capacity of 365 mg/g for Cr(VI), 469 mg/g for MB dye, and 317 mg/g for CR dye, respectively, while Fe_3O_4-OPBC-(CO_2) had a maximum adsorption capacity of 354 mg/g, 439 mg/g, and 299 mg/g, respectively. The excellent adsorption capacity for Cr(VI), MB, and CR dye was demonstrated by both Fe_3O_4-OPBC-NCs, although Fe_3O_4-OPBC-(N_2) exhibits better adsorption capacity; it was 3.05, 6.91, and 5.84 % for Cr(VI), MB dye, and CR dye more, respectively, than Fe_3O_4-OPBC-(CO_2). The adsorption efficiency of both NCs was minimally impacted by the presence of anions like PO_4^{3-} , SO_4^{2-} and SiO_3^{2-}. Moreover, after four cycles, the prepared NCs can exhibit high removal performance towards Cr(VI), CR, and MB dyes.

Batool et al. [94] synthesized zero-valent iron (Fe^0) supported on biochar nanocomposite and manufactured *N. lappaceum* (Rambutan) fruit peel waste-derived-biochar (B_{RtP}) for the removal of six specified organochlorine pesticides (OCPs) from an aqueous medium (Fe^0-B_{RtP}). The simple synthesis of Fe^0-B_{RtP}, which uses rambutan peel extract as the green reducing mediator to reduce Fe^{2+} to zero-valent iron, was carried out in place of the hazardous $NaBH_4$ that was employed for the chemical synthesis of Fe^0-B_{Che}, which is also synthesized for comparison purposes (Fe^0). Batch tests revealed that Fe^0-B_{RtP} and Fe^0-B_{Che} nanocomposites combine the benefits of adsorption and dechlorination of OCPs in the aqueous medium for OCPs (2 ppm) and 0.45 g/L as an adsorbent dosage at starting pH 4. Within 120 and 150 min, 83–91% and up to 96–99% elimination, respectively, were completed. The OCPs' adsorption isotherm closely matched the Langmuir isotherm, pointing to monolayer adsorption. After five cycles, the removal efficiencies of the regenerating Fe^0-B_{Che} and Fe^0-B_{RtP} were respectively 5–13% and 89–92%.

A biochar-based silver nanocomposite (Ag-nBC) was prepared by Shaikh et al. [95] by combining (i) AgNPs synthesized biochemically using *S. robusta* leaf extract and (ii) *S. robusta* leaf biochar produced through mild thermal pyrolysis (300 °C) for dye adsorption. The synthesized Ag-nBC was deemed to be stable, very porous, heterogeneous, and containing sizable amounts of the surface functional groups –OH, C–H, C=C, C=O, and C–O. AgNPs doping was found to considerably boost the dye adsorption capability of Ag-nBC by increasing the pore volume, specific surface binding sites, and most crucially, the surface area, which increased

by approximately 14 times over *S. robusta* leaf biochar. With maximum adsorption capacities of approximately 23.39 mg/g and 23.55 mg/g, respectively, removal percentages of RhB and CR were 93.57% and 94.18%, respectively. Exothermic and spontaneous chemisorption took place on the Ag-nBC surface, and the adsorption process involved many layers (Freundlich isotherm). For RhB adsorption, electrostatic attraction was used alone, whereas electrostatic attraction and H-bonding were used for the CR adsorption procedure. The extraordinary Ag-nBC reusability (> 70% after the third cycle and > 62% after the fifth cycle) has also been observed, proving the material's viability and lowering the overall cost of the treatment process.

For the adsorption of ketamine (KET), Liu et al. [96] prepared a nanocomposite comprising the metal-organic framework ZIF-8 and biochar that had been magnetically modified (MZBC). ZIF-8 was employed as a sacrifice template, and magnetic biochar (MBC) was prepared from pomelo peels. Investigations were done into how the performance of adsorption was affected by various pyrolysis temperatures (400, 500, 600, and 700 °C). For the production of MZBC, 600 °C was found to be the ideal pyrolysis temperature. The highest amount of KET that MZBC-600 could adsorb was 32.50 mg/g, which was 24.8 times more than what single magnetic biochar could adsorb (MBC-600). Over a broad pH (3–12) range and even at high ionic strength in solution, MZBC-600 demonstrated strong and stable adsorption capability for KET. The adsorption of KET on MZBC-600 was fitted to the Freundlich isotherm and the pseudo-second-order kinetic models. Pore filling, H—bonding, π-π and chelation interactions accounted for the majority of the adsorption process, as seen in Fig. 7. Even after five adsorption cycles, the MZBC-600 exhibited more than 90% of its initial adsorption capacity.

In some cases, changing the structure of BC might have an adverse effect on its characteristics (for example, lowering SSA), but it might also boost the potential of BC for the intended applications. Some studies have demonstrated that adding clay to the structure of BC diminishes the BC's accessible surface area, which is thought to be the key factor affecting the adsorbents' potential for pollutant adsorption capacity. The inclusion of clay may considerably boost the BC's power to adsorb heavy metals since clay-based materials (such as montmorillonite) have a high ion exchangeability for various cations [28].

5 Biochar-based nanocomposites as photocatalysts

The development of multifunctional materials that can entirely degrade different pollutants in wastewater is still a big challenge [97]. Yu et al. [98] used a simple ball-milling method to synthesize novel ZnO/bamboo-derived-biochar nanocomposites for MB dye removal. The weight ratio of ZnO is varied in the range of (0–75%). Ball milling broke down BC and ZnO, increasing the nanocomposites' mesopores and macropores. The photocatalytic and adsorption capacities of the nanocomposites for the removal of methylene blue (MB) were improved by adding 25% of ZnO to BC; when a composite is 1.8 g, the amount of ZnO is 0.45

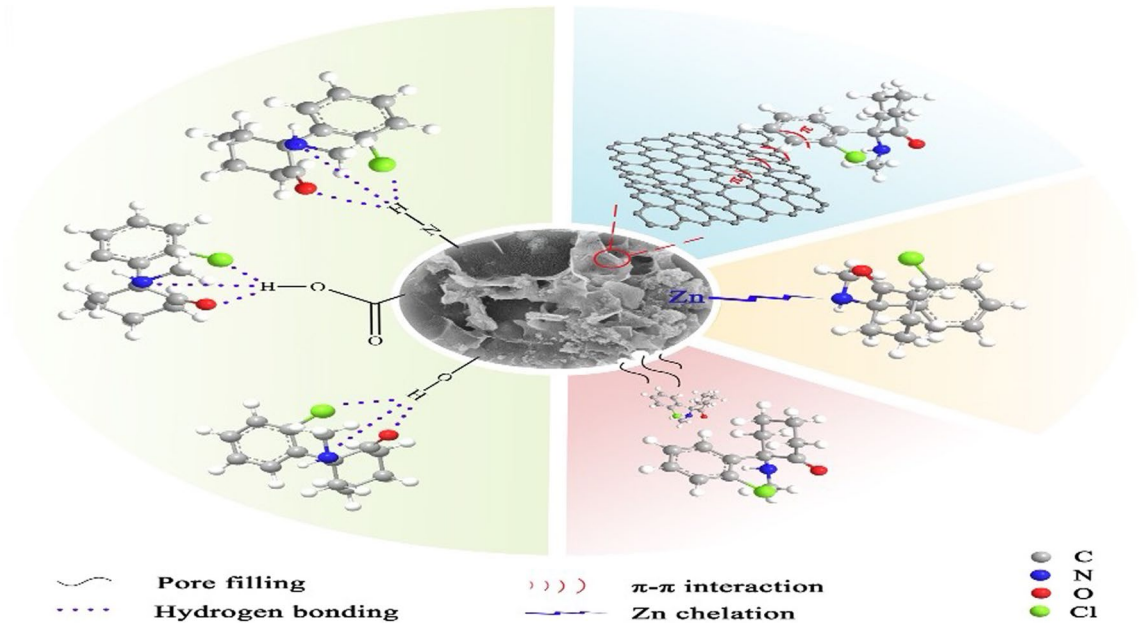

Fig. 7 Suggested adsorption mechanism for MZBC-600 towards KET [96]

g. By combining adsorption and photocatalysis, the nanocomposites demonstrated high MB removal effectiveness (up to 95.19%) for (25% ZnO/BC) under visible light when the initial MB concentration was equivalent to 160 ppm. The primary method of MB removal by ZnO/BC nanocomposites is adsorption, which is controlled by an electrostatic attraction mechanism (Fig. 8). However, the removal of MB from water by the nanocomposites may also depend on photocatalytic degradation. ZnO nanoparticles can efficiently produce free radicals to break down highly concentrated MB in water when exposed to visible light with the help of BC.

Kamal et al. [99] optimized the photocatalysis technique to degrade organic and inorganic pollutants under visible light irradiation. In which biochar with distinctive physicochemical properties was prepared from maize straw in a vacuum furnace. Also, ZnO-loaded maize biochar nanocomposite (MB-ZnO) for the photocatalytic degradation of Safranin O (Saf) and Mancozeb (MC) was synthesized by a solvent-free ball-milling method. The degradation of Saf by the MB-ZnO composite under visible light (83.5%), UV (81.0%), and darkness (78%) took place in one hour. The highest MC degradation by MB-ZnO nanocomposite was also observed by visible light (56.5 %), followed by UV radiation (27.5 %) and dark (25.2 %). The results of this investigation showed that, in both light and dark conditions, MB-ZnO nanocomposite might function as a superb catalyst to remove aqueous contaminants.

By using *Caragana korshinskii* biomass as the raw material for the biochar, Wang et al. [100] generated activated biochar (ACB), which was then combined with K^+ doped g-C_3N_4 (K-gC_3N_4) to form a composite material called ACB-K-gC_3N_4. There are different types of dye and antibiotic pollutants that are photodegraded utilizing this (ACB-K-gC_3N_4) composite include rhodamine B (RhB), tetracycline (TC), norfloxacin (NOR), and chloramphenicol (CAP). The results showed that K-gC_3N_4 and ACB could be successfully coupled, with the best results occurring at a loading mass ratio of 1:2. ACB-K-gC_3N_4 was superior than K-gC_3N_4 in terms of SSA, functional groups, band gap (2.29 eV), and visible light absorption (about 716 nm). With ACB-K-gC_3N_4, which had a degradation rate constant (0.0119 min^{-1}) four times higher than K-gC_3N_4 (0.0029 min^{-1}), RhB was eliminated with a 93.26% efficiency. $^{\cdot}O_2^-$, h^+, and $^{\cdot}OH$ were the primary photodegradation catalysts. This was explained by enhanced photogenerated carrier adsorption and transfer, easier production of active species, faster photogenerated electron migration, and reduced heterojunction recombination of photogenerated carriers. The peculiar surface characteristics (defects and lingering free radicals) and structure of ACB were attributed for these effects.

Fatimah et al. [101] prepared magnetic biochar photocatalyst (MBC) from snake fruit peel by immobilizing iron oxide precursors via co-precipitation followed by carbonization under N_2 gas at 400 °C for 2 h for photodegradation of rhodamine B (RhB). The obtained band gap energy is 2.23 eV, particle size ranging is at 5–20 nm, and the BET-specific surface area is 126 m^2/g which supports its photocatalytic activity for RhB photodegradation. Photodegradation of RhB followed second-order kinetics at the optimum pH of 7 and H_2O_2 concentration of 0.5% with the degradation efficiency of 99.9% for 15 min under UV light. The material exhibited good stability until the fifth cycle of usage, indicating that magnetic biochar with a low-cost feature has stability and the potential to be applied on a large scale.

In order to achieve synergistic adsorption and photocatalysis for MB and RhB, Cheng et al. [102] developed a new biochar/2$Zn_3In_2S_6$/WO_3 (BC/2ZIS/W) photocatalyst using the hydrothermal technique. The ZIS/W heterojunction had a large SSA (1161 m^2/g), good electrical conductivity, and was uniformly distributed over the carrier, which considerably improved the photocatalytic activity. The highest adsorption capacity of the BC/2ZIS/W for MB and RhB was found to be 120 and 466 mg/g, respectively, according to the adsorption isotherm. The removal of MB and RhB reached 80.5% and 99%, under the synergistic impact of adsorption

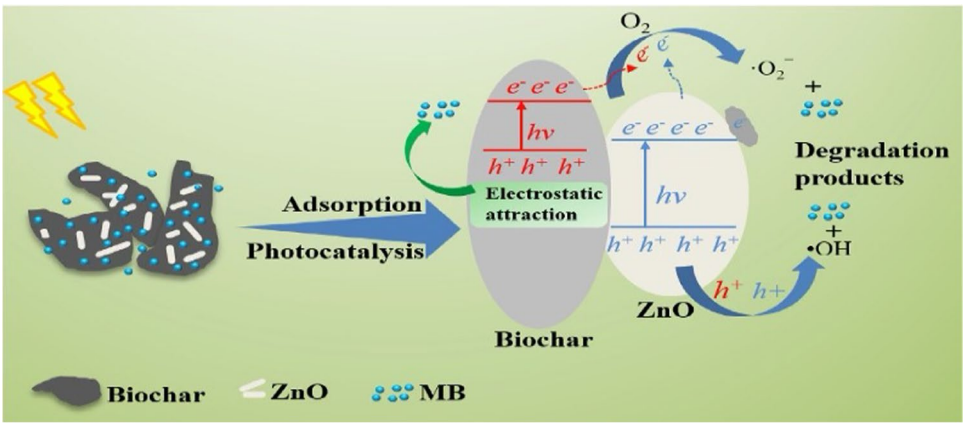

Fig. 8 Photocatalytic degradation of MB dye by ZnO/biochar under visible light [98]

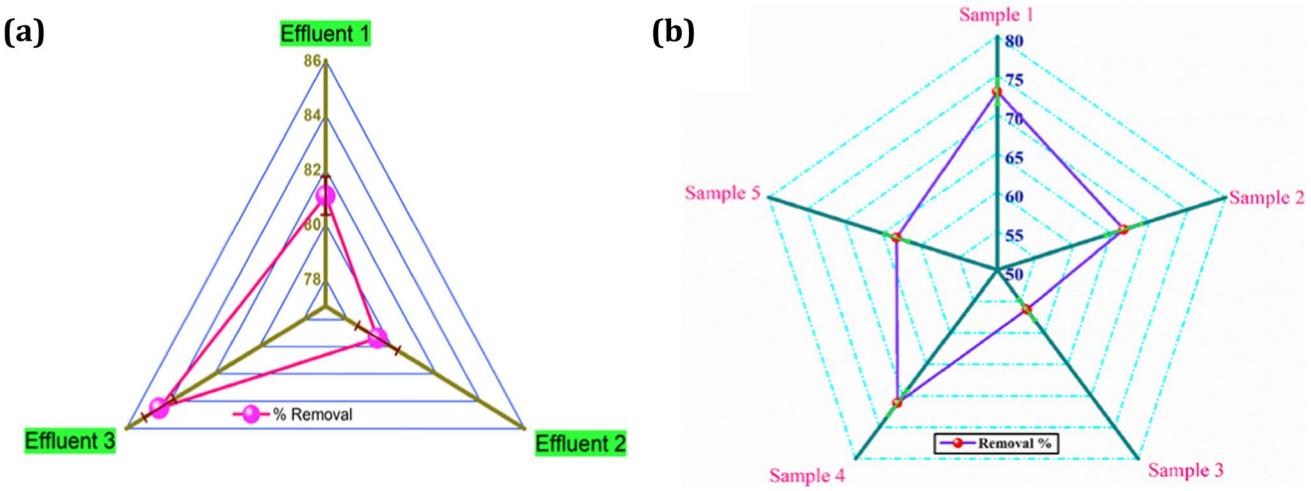

Fig. 9 Real treatment of dye textile wastewater using (**a**) Ag-nBC and (**b**) nAg-TC, where BC, *S. robusta* leaf biochar; TC, tea leaf biochar [95, 105]

and photocatalysis, which were noticeably higher than that of the single heterojunction.

Kang et al. [103] prepared composites of biochar modified with CdS and sulfur (CdS/S-BC) using the impregnation and calcination techniques. Due to the modification of S, biochar that has been treated with sulfur (S-BC) exhibits high porosity and a significant amount of SSA. For RhB dye, 1-CdS/S-BC (1 denotes the CdS molar amount) demonstrates strong synergistic adsorption-photocatalytic degradation (99.18%) after one hour under visible light. The exceptional RhB removal performance of 1-CdS/S-BC was not only attributed to the high SSA and plentiful reactive sites given by S-BC but may also greatly facilitate the migration and usage of photoinduced carriers. Superoxide radicals ($^{\cdot}O_2^-$) are the primary active species in the photocatalytic degradation process, according to the CdS/S-BC adsorption mechanism investigations, which showed that H–bond and electrostatic interaction are the key actions of adsorption.

By pyrolyzing the waste biomass from lychee peels, Siara et al. [104] prepared biochar-$ZnAl_2O_4$ composites for the adsorption and photocatalysis of ibuprofen as a model of pharmaceutical pollutants. In two hours (one-hour adsorption + one-hour photocatalysis), at pH = 6.5, 25 °C, and 1 g/L of the composite, the composite achieved 100% removal efficiency of (20 ppm) ibuprofen. The composite adsorption performance was greatly improved by the $ZnAl_2O_4$ support, and the biochar's mesoporous region, pore volume, and SSA (111 m^2/g) all worked together to promote the photocatalytic activity of $ZnAl_2O_4$, with k = 0.0093 min^{-1}. The ibuprofen's aqueous solution is photo catalytically degraded by the radicals $^{\bullet}OH$ and $O_2^{-\bullet}$. Due to the presence of functional groups on the biochar surface, which contribute to the reaction and prevent the recombination of the electron-hole pairs, the biochar-$ZnAl_2O_4$ composite demonstrated that the support of $ZnAl_2O_4$ in the biochar is required to boost photoactivity. The composite is also robust and functional even after six cycles, making it a suitable material for use in the removal of dangerous chemicals from wastewater.

6 Biochar-based nanocomposites for treatment of real wastewater

Dye effluents are a complex mixture of persistent organic pollutants (POPs), dissolved solids, wasted oil, and competitive ions, especially inorganic metal ions, which have a big impact on real effluent treatment [105]. Biochar-based nanocomposites are widely utilized in adsorption and photocatalytic degradation because of their excellent physical and chemical features, including improved porosity, high SSA, rich surface functional groups, and great reusability (including dyes, phenols, heavy metals, pharmaceuticals, and so on). These characteristics have led to the usage of biochar-based nanocomposites to cope with and eliminate hazardous dyes through adsorption from synthetic solutions and real wastewater in various research.

Shaikh et al. [95] used the chemical co-precipitation method to dope AgNPs onto *S. robusta* leaf biochar (Ag-nBC) for RhB and CR dyes adsorption, where the AgNPs were homogeneously distributed on the composite matrix. Maximum removal efficiencies of RhB and CR at equilibrium were attained using batch mode adsorption and were > 90%. At the optimum conditions (Ag-nBC dose 0.8 g/L, 27 °C, 300 rpm as stirring rate, pH 7, and contact time = 50 min), real effluent samples, however, demonstrated 7–12% lower efficiency (Fig. 9(a)). The inorganic metals in the effluents, which competed with dye molecules and/or blocked the available pores and binding sites on

the composite surface, may be responsible for this loss in efficiency [106, 107].

Additionally, Shaikh et al. [105] prepared 'Tea leaf biochar' (TC) from tea leaf waste and fabricated a hybrid nanocomposite (nAg-TC) with colloidal deposition of silver nanoparticles (nAg) via modified chemical co-precipitation. With dye concentrations of 72.9 mg/L (sample 1), 66.7 mg/L (sample 2), 56.3 mg/L (sample 3), 71.1 mg/L (sample 4), and 63.2 mg/L (sample 5), the produced nAg-TC is examined for its practical implications for the treatment of five real textile effluents. These real textile effluents had adsorption efficiencies ranging from 21.2 to 39.6%, which was lower than the adsorption efficiency attained during the equilibrium adsorption of synthetic RhB and CR solutions (Fig. 9(b)). Due to the presence of competing ions, high concentrations of dissolved solids, and other persistent contaminants, which hindered the nAg-TC matrix's active binding sites, the dye removal efficiencies may have been decreased [107]. But compared to other experiments utilizing conventional bio-adsorbents, the dye removal efficiency was higher. The significant characteristics of the nAg-TC matrix were responsible for the study's improved dye removal efficiency. The main benefit of nAg-TC is a result of the synergistic actions of nAg and TC, which led to increased porosity, a high SSA, and a rich active functional group content with outstanding reusability [105].

Wang et al. [100] investigated the applicability of ACB-K-gC_3N_4 for real wastewater treatment. Five samples from the Yellow River, Weihe River, wastewater A (from textile factory), wastewater B (from rabbit breeding factory), and wastewater C (from chicken factory) were used. By using ACB-K-gC_3N_4, the complete degradation of RhB for samples taken from the Weihe River and the Yellow River is achieved after 5 min, while for Wastewater A only 79 % is degraded at 180 min (Fig. 10a). This is because the concentration of RhB in the sample from the Yellow River was very low and was not found in the sample from the Weihe River, allowing ACB-K-gC_3N_4 to quickly and entirely eliminate RhB. Wastewater A has a high BOD and COD together with poor biodegradability [108]. The promise of ACB-K-gC_3N_4 for advanced oxidation treatment can be shown despite the fact that the photocatalytic activity of ACB-K-gC_3N_4 was somewhat hindered by the potential existence of interfering ions in wastewater A. ACB-K-gC_3N_4 also completely degraded the TC of two surface water samples from the Weihe River and Yellow River at 10 min, while degraded only 72% and 76% from wastewater B and wastewater C samples, respectively, at 180 min (Fig. 10b). The BOD and COD concentrations of wastewater B and wastewater C were both very high, and wastewater B also had very low biodegradability. Furthermore, wastewater B and C samples contained NOR and CAP pollutants. Unexpectedly, it was discovered that ACB-K-gC_3N_4 achieved removal efficiencies of 56 and 51 % for NOR and CAP in wastewater B and 61 and 65 % for NOR and CAP in wastewater C, respectively. This suggested that ACB-KgC_3N_4 may manage several antibiotics concurrently in a complex contaminated environment. Fortunately, the investigation showed that the real wastewater was successfully treated, which positively illustrated the viability of using ACB-K-gC_3N_4 to treat a high amount of real wastewater.

7 Parameters affecting the adsorption and photocatalytic degradation processes

This section looked into a variety of parameters, including the adsorbent/photocatalyst dose, the initial pollutant concentration, temperature, the pH of the solution, the presence of scavengers and anions, etc. (Fig. 11). Practically, it is essential to understand the effect of these parameters on the adsorption and photocatalytic degradation processes

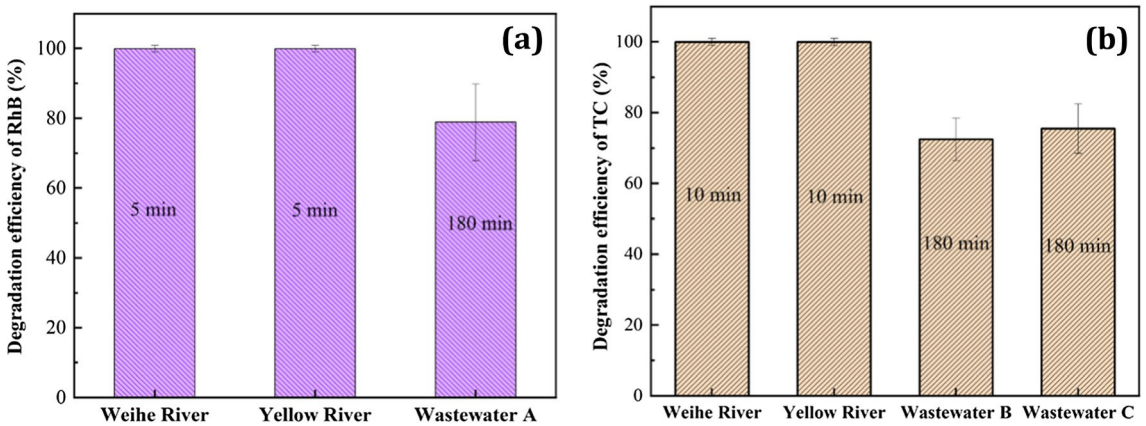

Fig. 10 Real industrial wastewater tests of photocatalytic degradation for RhB (**a**) and TC (**b**). (dose = 1 g/L, 500 W xenon lamp) [100]

in order to design an effective economic adsorption/photoreactor system.

7.1 Effect of adsorbent/photocatalyst dose

The most significant parameter influencing the adsorption/photocatalytic activity is thought to be the adsorbent/photocatalyst dose. To prevent any additional dose, it is crucial to maximize the adsorbent/photocatalyst dose during the removal process. The reaction must be as efficient as possible while using the least amount of adsorbent/photocatalyst possible in order to be economically viable. The removal efficiency rises together with increasing the adsorbent/photocatalyst dose due to the presence of more active sites on its surface. As a result, a large quantity of $^{\bullet}OH$ and other ROS will be produced, which is what actually degrades organic contaminants. In contrast, using too much photocatalyst will limit the photocatalytic degradation activity and cause the reactor to become hazy, which lowers light passing through the solution [109, 110].

According to Sun et al. [111], the decrease in photoactive surface area and rise in nanoparticle aggregation caused by a photocatalyst dose increase over the optimal value will decrease the degradation efficiency. According to Riga et al. [112], increasing the photocatalyst dose increases the amount of dye adsorbed on TiO_2. The impact of the photocatalyst dose on the photocatalytic degradation performance using several photocatalysts is shown in Fig. 12. By applying different doses (0.5–1.5 g/L) of Fe_3O_4@SiO_2@$PTSiMo_{12}$ photocatalyst, Fig. 12 a demonstrates the photocatalytic oxidative desulfurization (ODS) in the gasoline fuel [113].

After 45 minutes of illumination, Jabbar and Ebrahim [114] showed that increasing the dose of $SiO_2/Fe_3O_4/Ag_2WO_4$ from 0.5 to 1 g/L resulted in a 75–88% increase in the photocatalytic degradation efficiency of MB dye. The rise in the generation of the photogenerated electron-hole pairs is responsible for this (Fig. 12b).

Nadeem et al. [115] carried out a different experiment employing different doses of CFA/$ZnFe_2O_4$ (coal fly ash-based zinc ferrite) composite as a photocatalyst for MB dye (20–200 mg/L). Due to the photocatalyst agglomeration and the release of Fe^{2+} that scavenge the generated $^{\bullet}OH$, they found that raising the photocatalyst dose over 110 mg/L decreases removal efficiency (Fig. 12c).

7.2 Effect of pollutant concentration

Another significant parameter that affects the removal of harmful chemicals and dyes is the pollutant concentration in the solution. Most removal studies chose the pollutant concentration between 10 and 200 ppm to simulate the concentrations of these pollutants that are released into discharged industrial effluent. When colored substances like dyes are present at higher concentrations, photocatalytic degradation efficacy against them improves; nevertheless, once a certain concentration is reached, it starts to decline. This is explained by the fact that before reaching the photocatalyst surface, the dye molecules will screen the UV-visible light that has been exposed [116].

According to Liu et al. [117], raising the bisphenol A (BPA) concentration from 5 to 20 ppm resulted in a reduction in the photocatalytic degradation activity

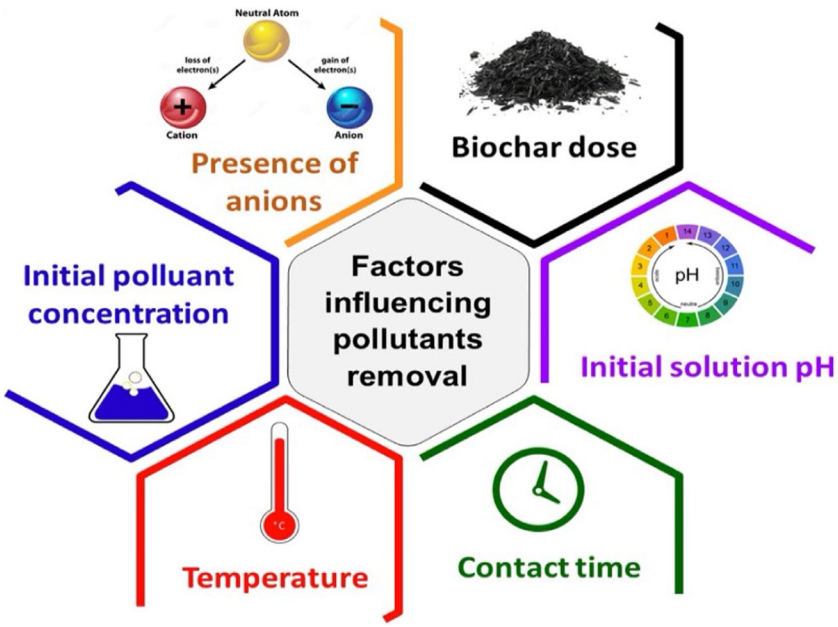

Fig. 11 Parameters affecting the removal of pollutants [18]

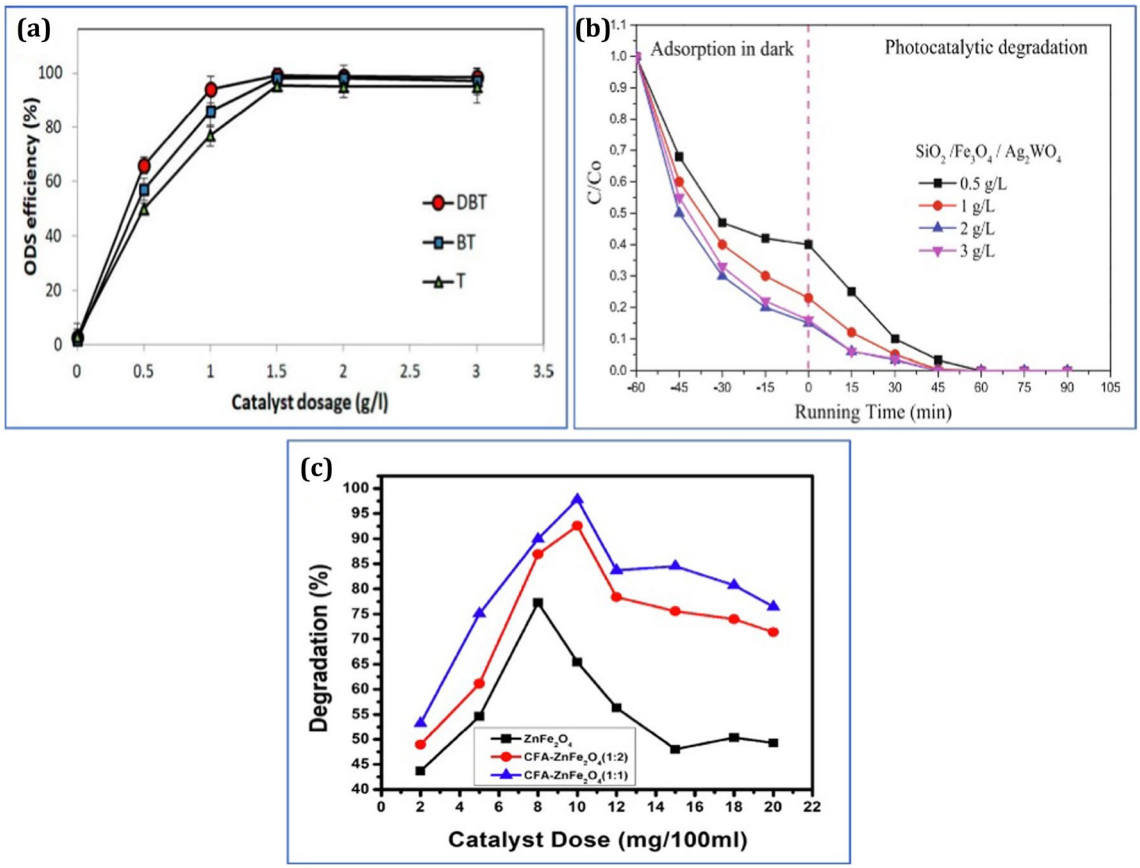

Fig. 12 (**a**) Effect of Fe_3O_4@SiO_2@PT\$SiMo_{12}$ dose on the photocatalytic degradation of ODS (40 °C, sulfur conc. = 250 ppm, time = 60 min) [113], (**b**) Photodegradation of MB with different doses of SiO_2/Fe_3O_4/Ag_2WO_4 (pH 11, [MB] = 30 ppm) [114], (**c**) MB dye degradation at different doses (20–200 mg/L) of CFA/$ZnFe_2O_4$ [115]

of PS/g-C_3N_4 nanosheets from 100% to 70%, respectively. This decrease in the photocatalytic degradation efficiency is due to the competition between BPA molecules for active sites on the PS/g-C_3N_4 nanosheet surface. When Zheng et al. [118] employed the flower-like MgO as a photocatalyst for MB degradation under UV light irradiation, a similar result was observed. It was discovered that the degradation efficiency could reach 99% when 100 mg/L of MB is irradiated for 24 min. With 500 mg/L MB concentration, this degradation efficiency was drastically decreased over the course of 315 minutes to 18.74% (Fig. 13a). Additionally, the absence of appropriate active species ($^{\bullet}OH$, $^{\bullet}O_2^{-}$, H_2O_2, h_{VB}^{+}), which are required to react with the high pollutant concentration, may also be the cause of the decreased degradation rate. Chu et al. [119], who evaluated the impact of the initial BPA concentration (5–30 mg/L) on the BPA degradation activity using Bi_2O_3/SnO_2 photocatalyst under solar light irradiation, observed this outcome. At low initial concentrations (5 mg/L), higher degradation rates were observed in a shorter amount of time (Fig. 13b). This is due to the high rate of light penetration, which causes a significant number of active species to be generated at a low pollutant concentration.

7.3 Effect of pH

pH value is quite important as it seems to have a significant impact on the surface charge of adsorbents, the morphologies of metal species, and the degree of protonation of surface functional groups. When pH falls below pH_{pzc} (point of zero charge), a lot of H^+ or H_3O^+ ions fill the active sites and form positively charged adsorbents, which reduce the removal efficiency by weakening the functional groups and producing electric repulsion to divalent metal ions with positive charges. When pH was greater than pH_{pzc}, heavy metal species with positive charges in water were clearly attracted by electrostatic forces to biochar with negatively charged surfaces [120]. Additionally, as pH increased, the protonation degree of the materials dropped, enabling a high amount of oxygen- and nitrogen-containing adsorption sites to easily fill in the empty orbits of heavy metal ions and significantly enhancing (magnetic biochar) MBC adsorption ability. For instance, Cr (VI) typically appears as $HCrO_4^-$ and

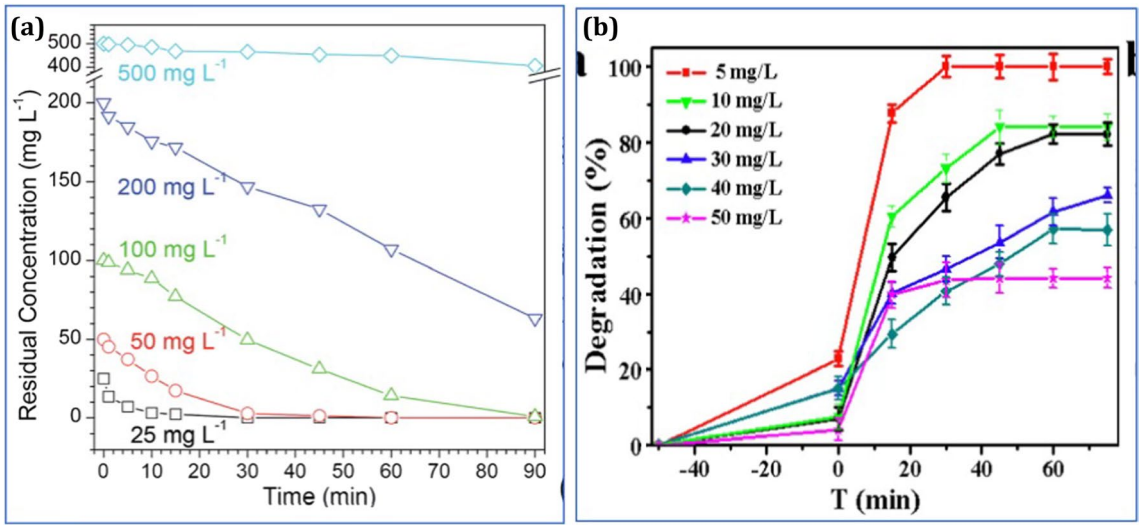

Fig. 13 (**a**) The photocatalytic behavior of MgO for degradation of MB dye (25–500 mg/L) [118], (**b**) The degradation activity of Bi_2O_3/SnO_2 for degradation of BPA (5–50 mg/L) under solar light [119]

$Cr_2O_7^{2-}$ between pH 1.0 and 6.0, and CrO_4^{2-} above pH 6. Because more $HCrO_4^-$ and $Cr_2O_7^{2-}$ were formed at low pH levels, the interaction between the positively charged functional groups of the adsorbent and the negatively charged chromate ions was strengthened. As a result, the greater Cr(VI) adsorption performances were significant. Due to the competitive adsorption of Cr(VI) with hydroxide complexes, Cr(VI) removal capacity reduced as pH increased [121].

Taking into account, increasing pH may cause precipitation of metal ions which depends on the specific metal ion and the solution conditions. Generally, the formation of insoluble hydroxide or oxide precipitates, can decrease the solubility of metal ions with increasing pH. As the pH increases, the concentration of hydroxide ions in the solution also increases, and if the concentration of metal ions exceeds their solubility limit, insoluble hydroxide precipitates can form and settle out of solution. For instance, some metal ions such as aluminum, chromium, iron, and zinc can form hydroxide precipitates at high pH values.

Furthermore, because industrial wastewater has a range of pHs, it is important to investigate how pH affects the response of the removal processes. The photocatalyst surface characteristics and the structure of the target pollutants are all affected by the solution pH, which can have an impact on the catalytic performance. As a result, by regulating the surface charges of the adsorbent/photocatalyst and the contaminant, the pH of the reaction influences the photocatalytic reaction and, consequently, the adsorption of the pollutants on the photocatalyst's surface. The point of zero charge of the photocatalyst (pH_{pzc}) should be determined in order to evaluate the impact of pH on the surface charge. Because of this, the photocatalyst has a (+) charge at pH levels below pH_{pzc} and a (-) charge at pH levels above pH_{pzc} [122].

ZVZ-g-C_3N_4 (zero-valent zinc immobilized g-C_3N_4) was used to catalyze the ozonation process in the atrazine (ATZ) degradation, and Yuan et al. [123] investigated the impact of pH on this process. The pH_{pzc} of the ZVZ-g-C_3N_4 was found to be 5.96. Due to its negative charge in the pH range (7 – 9), the ZVZ-g-C_3N_4 catalyst demonstrated better ATZ degradation efficacy.

Li et al. [124] made another contribution by using $FeCo_2S_4$/g-C_3N_4 for the degradation of sulfamethoxazole (SMX). $FeCo_2S_4$/g-C_3N_4 has a pH_{pzc} value of 5.9, meaning that the surface charge is positive between 3.5 and 5.0 and negative between 6.5 and 9.5. Since the SMX persisted as an anionic species at a high pH range, improving the adsorption between the SMX and $FeCo_2S_4$/g-C_3N_4 and promoting the degradation performance, the perforable degradation was discovered at an initial pH value of (3.5–5.0).

7.4 Effect of interfering ions

Generally, wastewater contains large amounts of salts, and the water body is recognized to be a complicated system [125]. In order to effectively remove pollutants from wastewater, it is important to consider the ionic strength of the solution. According to Sun et al. [126] anions have an impact on how well Cr(VI) is adsorbed in wastewater. Adsorption tests showed that the presence of Cl^-, NO_3^-, $H_2PO_4^-$ and HPO_4^{2-} slightly decreased the adsorption efficiency. At 150 and 300 ppm co-existing anion concentrations, respectively, the efficiency losses were smaller than 2.6% and 7.3%. However, the presence of SO_4^{2-} significantly reduced the ability of Cr(VI) adsorption, with efficiency losses of up to 18.5 and 23.7 % at the same two concentrations.

Qu et al. [127] also examined the effects of co-existing anions, such as SO_4^{2-}, NO_3^-, CO_3^{2-}, HCO_3^- and Cl^- on P adsorption by La-Fe-BC at low (0.01 M) as well as high (0.1 M) concentrations. The decrease in adsorption performance implied that CO_3^{2-} and HCO_3^- had significant effects on P adsorption. As a result, competing ions in the solution have the ability to alter the surface characteristics of adsorbents in addition to limiting activated adsorption sites. Additionally, as ionic strength rises, the electrostatic attraction between the pollutants that have been adsorbed weakens, lowering the ability of contaminants to be removed.

7.5 Effect of contact time

The evaluation of the adsorption/photodegradation of biochar must take the impact of contact time into account. According to published research, the removal capacity rapidly increases at the start of the treatment before gradually decreasing until adsorption equilibrium is reached, at which point the sorption sites are completely filled. This can be explained by the gradual saturation of active sites by adsorption on biochar and the gradual decline in the differential concentration between the surface of the adsorbent and the bulk phase of the solution [128]. Similar outcomes were observed by Sayin et al. [129] in their study on the elimination of ciprofloxacin by H_3PO_4 modified biochar. They stated that the rate of antibiotic molecule adsorption decreased with increasing treatment time and that this continued until the point of equilibrium. For the purpose of removing the Congo red dye, Nguyen et al. [130] investigated various metal salt-modified biochars made from various agricultural wastes. The outcomes showed that various biochars applied at the same initial dye concentration required various equilibrium times (Fig. 14).

7.6 Effect of reaction temperature

The adsorption/photocatalytic degradation process of contaminants is clearly associated with raising the reaction temperature. The adsorption/photocatalytic activity is enhanced as a result of the increase in reaction temperature, which increases the creation of reactive radicals brought on by the formation of bubbles during the photoreaction process. Additionally, a rise in temperature can accelerate degradation by slowing the recombination of e^-/h^+ pairs. Furthermore, the interface can acquire a substantial deterioration rate [131].

Batool et al. [94] prepared *N. lappaceum* (Rambutan) fruit peel waste-derived-biochar (B_{RtP}) and synthesized zero-valent iron (Fe^0) supported on biochar nanocomposite (Fe^0-B_{RtP}) for the removal process of organochlorine pesticides (OCPs). They studied the effect of different parameters

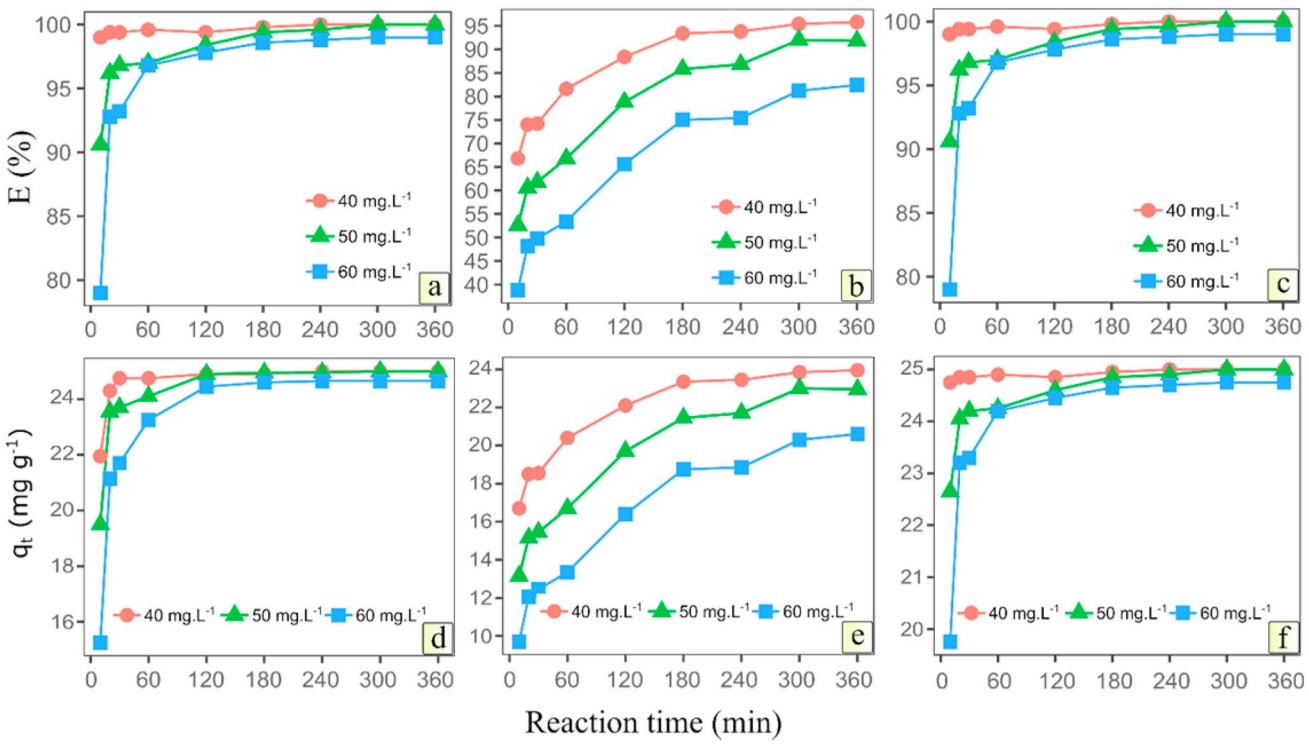

Fig. 14 Effect of reaction time on CR removal in terms of percentage and adsorption capacity at initial concentration of 40–60 mg/L of $AlCl_3$-biochar (**a**, **d**), $CaCl_2$- biochar (**b**, **c**), and $FeCl_3$-biochar (**c**, **f**) [130]

such as pH, adsorbent dose, initial pollutant concentration, time and temperature on the removal of OCPs using the prepared Fe^0-B_{RtP}. it is found that the optimum parameters are pH = 4, 0.45 g/L as adsorbent dose, 2 mg/L as initial pesticides concentration, and the equilibrium time is in the range (120–150 min). Besides, it is mentioned that increasing the temperature from 25 °C up to 45 °C accelerates the removal of pollutants may be due to the increased movement of the OCPs molecules from a liquid medium to a nano-adsorbent surface.

7.7 Effect of running cycles

In order to determine the practical applicability and check the stability during adsorption/photocatalytic degradation processes, it is crucial to analyze the adsorption/photocatalytic activity in numerous subsequent running cycles. The stability test is vital to prevent the subsequent contamination of treated water caused by metals released during the adsorption/photocatalytic reactions. It is possible to conduct the stability and reusability tests three, four, or five times in succession. The adsorbent/photocatalyst is separated, repeatedly rinsed with ethanol or deionized H_2O, and dried at 105 °C for the subsequent application after each cycle [132]. For instance, BC-TiO_2 nanocomposites may be reused and recycled up to five or six times with a high removal efficiency. In some cases, even after the fifth cycle, substantial photocatalytic efficiencies have been seen for the degradation of pollutants, as in the case of Zhang et al. [133], who found photocatalytic efficiencies of more than 85% after five successive cycles.

8 Conclusion

In recent years, there has been a lot of interest in BC and BC-based nanocomposites for a variety of applications, particularly for pollutants removal. With growing concerns about the practical application of BC-based nanocomposites for wastewater treatment by various processes, this review sheds light on these nanocomposites, their preparation methods, and their critical role in wastewater treatment via adsorption and photocatalytic degradation processes. The fabrication of BC and BC-based nanocomposites from biomass was summarized in this review. To prepare BC, pyrolysis, hydrothermal carbonization, torrefaction, and gasification are used, whereas sol-gel, ultrasonication, and hydrothermal are used for BC-based nanocomposites. These BC-based nanocomposites have inherent properties that help to overcome the practical limitations of pristine BC and photocatalysts. High adsorption and photocatalytic activity, improved reusability, and simplified recovery were achieved by the BC-based nanocomposites. Furthermore, the band gap energies and recombination rates of electron-hole pairs in BC-based nanocomposites were reduced, which is desirable for photocatalytic applications. The surface areas of the composites, on the other hand, are typically smaller than those of the pristine BC but greater than those of the pristine photocatalysts. In practice, these nanocomposites outperform their pristine counterparts. The presence of biochar as an adsorbent and supportive material on the composite surface improves the adsorption of pollutants on the composite surface, which in turn improves the photocatalytic degradation of the pollutant, resulting in improved removal efficiency using these composites. Furthermore, in these composites, the photocatalytic part (e.g., metal oxide) acts as an electron donor, while the biochar part acts as an electron acceptor, promoting the separation of the electron-hole pairs. By using BC-based nanocomposites, various pollutant groups such as dyes, pharmaceutical compounds, and phenols were significantly degraded. Following that, the parameters affecting the performance of the removal processes, such as biochar dose, initial pollutant concentration, pH, time, temperature, the presence of various interfering anions, and recycling, were discussed and discovered to have a significant impact on the mentioned processes. This review provided a thorough understanding of the use of BC-based nanocomposites as effective adsorbents/photocatalysts with low-cost and high-performance properties for wastewater pollution remediation.

9 Challenges and future directions

For large-scale environmental applications, the scientific community is currently focusing on the development of sustainable materials that are effective, affordable, ecologically friendly, and socially acceptable. In this context, BC was mostly generated from waste biomass, which during the heating process could release harmful chemicals. As a result, in order to achieve effective recovery and large-scale commercial production of BC, the material preparation process needs to be improved. In order to increase the usage of BC-based nanocomposites for wastewater treatment applications, future research should concentrate on increasing the surface stability of the metal in the composites to decrease metal leaching as well as exploring affordable, effective, and environmentally friendly batch preparation technologies for these composites. The majority of research focused on the degradation or adsorption of just one pollutant, as this review has shown. The treatment of wastewater containing numerous pollutants through adsorption and photocatalysis should be studied in the future, as well as how organic matter from the environment affects photocatalytic processes in actual wastewater samples. Moreover, the large-scale manufacture of BC/BC-based nanocomposites and their useful

applications for wastewater treatment in developing nations worldwide are particularly promising.

Author contributions *Enas Amdeha:* Conceptualization, Writing - original draft, editing and reviewing.

Funding Open access funding provided by The Science, Technology & Innovation Funding Authority (STDF) in cooperation with The Egyptian Knowledge Bank (EKB).

Data availability All obtained data during this work are included in this manuscript.

Declarations

Ethical approval The manuscript is prepared in compliance with the Publishing Ethics Policy.

Competing interests The authors declare no competing interests.

References

1. Naidu R, Biswas B, Willett IR et al (2021) Chemical pollution: a growing peril and potential catastrophic risk to humanity. Environ Int 156:106616. https://doi.org/10.1016/j.envint.2021.106616
2. Sanganyado E (2022) Policies and regulations for the emerging pollutants in freshwater ecosystems: challenges and opportunities. Emerg Freshw Pollut:361–372. https://doi.org/10.1016/b978-0-12-822850-0.00007-7
3. Adeola AO, Abiodun BA, Adenuga DO, Nomngongo PN (2022) Adsorptive and photocatalytic remediation of hazardous organic chemical pollutants in aqueous medium: A review. J Contam Hydrol 248:104019. https://doi.org/10.1016/j.jconhyd.2022.104019
4. Mukherjee A, Dhak P, Hazra V et al (2023) Synthesis of mesoporous Fe/Al/La trimetallic oxide for photodegradation of various water-soluble dyes: kinetic, mechanistic, and pH studies. Environ Res 217:114862. https://doi.org/10.1016/j.envres.2022.114862
5. Mukherjee A, Panda B, Mondal D et al (2023) Mesoporous, phase-pure Al^{3+}engrafted spinel $ZnAl_xB_{2-x}O_4$ (X= 0, 1; B = Cr^{3+}/Fe^{3+}) for effective fluoride chemisorption and photodegradation of azo/non-azo dyes. J Environ Chem Eng 11:109237. https://doi.org/10.1016/j.jece.2022.109237
6. Amdeha E (2021) Recovery of nanomaterials from agricultural and industrial wastes for water treatment applications. In: Makhlouf ASH, Ali GAM (eds) Topics in Mining, Metallurgy and Materials Engineering. Springer, Cham, pp 385–417. https://link.springer.com/chapter/10.1007/978-3-030-68031-2_14
7. Wallerstein D (2020) Food-energy-water (FEW) nexus: rearchitecting the planet to accommodate 10 billion humans by 2050. Resour Conserv Recycl 155:104658. https://doi.org/10.1016/j.resconrec.2019.104658
8. Chen DMC, Bodirsky BL, Krueger T et al (2020) The world's growing municipal solid waste: trends and impacts. Environ Res Lett 15:074021. https://doi.org/10.1088/1748-9326/ab8659
9. Abou-Hadid AF, El-Behairy UA, Elmalih MM et al (2022) Production of efficient carbon fiber from different solid waste residuals for adsorption of hazardous metals from wastewater samples. Biomass Convers Biorefinery 1:1–16. https://doi.org/10.1007/s13399-022-03097-6
10. Abou-Hadid AF, El-Behairy UA, Elmalih MM et al (2023) Conversion of corn shell as biomass solid waste into carbon species for efficient decontamination of wastewater via heavy metals adsorption. Biomass Convers Biorefinery 1:3. https://doi.org/10.1007/s13399-023-04057-4
11. Uday V, Harikrishnan PS, Deoli K et al (2022) Current trends in production, morphology, and real-world environmental applications of biochar for the promotion of sustainability. Bioresour Technol 359:127467. https://doi.org/10.1016/j.biortech.2022.127467
12. Luo K, Pang Y, Wang D et al (2021) A critical review on the application of biochar in environmental pollution remediation: role of persistent free radicals (PFRs). J Environ Sci (China) 108:201–216. https://doi.org/10.1016/j.jes.2021.02.021
13. Li X, Zhang J, Liu B, Su Z (2021) A critical review on the application and recent developments of post-modified biochar in supercapacitors. J Clean Prod 310:127428. https://doi.org/10.1016/j.jclepro.2021.127428
14. Song B, Lin R, Lam CH et al (2021) Recent advances and challenges of inter-disciplinary biomass valorization by integrating hydrothermal and biological techniques. Renew Sustain Energy Rev 135:110370. https://doi.org/10.1016/j.rser.2020.110370
15. Li Y, Xing B, Ding Y et al (2020) A critical review of the production and advanced utilization of biochar via selective pyrolysis of lignocellulosic biomass. Bioresour Technol 312:123614. https://doi.org/10.1016/j.biortech.2020.123614
16. Tomczyk A, Sokołowska Z, Boguta P (2020) Biochar physicochemical properties: pyrolysis temperature and feedstock kind effects. Rev Environ Sci Biotechnol 19:191–215. https://doi.org/10.1007/s11157-020-09523-3
17. Jeyasubramanian K, Thangagiri B, Sakthivel A et al (2021) A complete review on biochar: production, property, multifaceted applications, interaction mechanism and computational approach. Fuel 292:120243. https://doi.org/10.1016/j.fuel.2021.120243
18. Zeghioud H, Fryda L, Djelal H et al (2022) A comprehensive review of biochar in removal of organic pollutants from wastewater: characterization, toxicity, activation/functionalization and influencing treatment factors. J Water Process Eng 47:102801. https://doi.org/10.1016/j.jwpe.2022.102801
19. Pan X, Gu Z, Chen W, Li Q (2021) Preparation of biochar and biochar composites and their application in a Fenton-like process for wastewater decontamination: a review. Sci Total Environ 754:142104. https://doi.org/10.1016/j.scitotenv.2020.142104
20. Rangarajan G, Jayaseelan A, Farnood R (2022) Photocatalytic reactive oxygen species generation and their mechanisms of action in pollutant removal with biochar supported photocatalysts: A review. J Clean Prod 346:131155. https://doi.org/10.1016/j.jclepro.2022.131155
21. Singh P, Mukherjee A, Mahato A et al (2022) A review on chemoselective reduction of nitroarenes for wastewater remediation using biochar supported metal catalysts: kinetic and mechanistic

studies. Chem Africa 6:561–578. https://doi.org/10.1007/s42250-022-00534-x
22. Xiao R, Luo Z, Wei Z et al (2018) Activation of peroxymonosulfate/persulfate by nanomaterials for sulfate radical-based advanced oxidation technologies. Curr Opin Chem Eng 19:51–58. https://doi.org/10.1016/j.coche.2017.12.005
23. Deng R, Huang D, Zeng G et al (2019) Decontamination of lead and tetracycline from aqueous solution by a promising carbonaceous nanocomposite: Interaction and mechanisms insight. Bioresour Technol 283:277–285. https://doi.org/10.1016/j.biortech.2019.03.086
24. Naushad M, Sharma G, Alothman ZA (2019) Photodegradation of toxic dye using Gum Arabic-crosslinked-poly(acrylamide)/$Ni(OH)_2$/FeOOH nanocomposites hydrogel. J Clean Prod 241:118263. https://doi.org/10.1016/j.jclepro.2019.118263
25. Kim S, Nam SN, Jang A et al (2022) Review of adsorption–membrane hybrid systems for water and wastewater treatment. Chemosphere 286:131916. https://doi.org/10.1016/j.chemosphere.2021.131916
26. Fito J, Kefeni KK, Nkambule TTI (2022) The potential of biochar-photocatalytic nanocomposites for removal of organic micropollutants from wastewater. Sci Total Environ 829:154648. https://doi.org/10.1016/j.scitotenv.2022.154648
27. Rajapaksha AU, Chen SS, Tsang DCW et al (2016) Engineered/designer biochar for contaminant removal/immobilization from soil and water: potential and implication of biochar modification. Chemosphere 148:276–291. https://doi.org/10.1016/j.chemosphere.2016.01.043
28. Kamali M, Appels L, Kwon EE et al (2021) Biochar in water and wastewater treatment - a sustainability assessment. Chem Eng J 420:129946. https://doi.org/10.1016/j.cej.2021.129946
29. Daful AG, R Chandraratne M (2020) Biochar production from biomass waste-derived material. Encycl Renew Sustain Mater 370–378. https://doi.org/10.1016/b978-0-12-803581-8.11249-4
30. Vieira FR, Romero Luna CM, Arce GLAF, Ávila I (2020) Optimization of slow pyrolysis process parameters using a fixed bed reactor for biochar yield from rice husk. Biomass Bioenergy 132:105412. https://doi.org/10.1016/j.biombioe.2019.105412
31. Ying ZX, Xie F, Jiang M et al (2021) Physicochemical properties and lead ion adsorption of biochar prepared from Turkish gall residue at different pyrolysis temperatures. Microsc Res Tech 84:1003–1011. https://doi.org/10.1002/jemt.23661
32. Kim JS (2015) Production, separation and applications of phenolic-rich bio-oil - a review. Bioresour Technol 178:90–98. https://doi.org/10.1016/j.biortech.2014.08.121
33. Dahou T, Defoort F, Khiari B et al (2021) Role of inorganics on the biomass char gasification reactivity: a review involving reaction mechanisms and kinetics models. Renew Sustain Energy Rev 135:110136. https://doi.org/10.1016/j.rser.2020.110136
34. Pauline AL, Joseph K (2020) Hydrothermal carbonization of organic wastes to carbonaceous solid fuel – a review of mechanisms and process parameters. Fuel 279:118472. https://doi.org/10.1016/j.fuel.2020.118472
35. Zhou X, Chen F, Bai T et al (2016) Interconnected highly graphitic carbon nanosheets derived from wheat stalk as high performance anode materials for lithium ion batteries. Green Chem 18:2078–2088. https://doi.org/10.1039/c5gc02122g
36. Hamid Y, Liu L, Usman M et al (2022) Functionalized biochars: Synthesis, characterization, and applications for removing trace elements from water. J Hazard Mater 437:129337. https://doi.org/10.1016/j.jhazmat.2022.129337
37. Yusup S, Yiin CL, Tan CJ, Abdullah B (2015) Determination of optimum condition for the production of rice husk-derived bio-oil by slow pyrolysis process. Process Dev Resour Conserv Biomass Convers:329–340. https://doi.org/10.1002/9781118699140.ch13
38. Chen WH, Peng J, Bi XT (2015) A state-of-the-art review of biomass torrefaction, densification and applications. Renew Sustain Energy Rev 44:847–866. https://doi.org/10.1016/j.rser.2014.12.039
39. Liu Z, Han G (2015) Production of solid fuel biochar from waste biomass by low temperature pyrolysis. Fuel 158:159–165. https://doi.org/10.1016/j.fuel.2015.05.032
40. Lu H, Zhang W, Wang S et al (2013) Characterization of sewage sludge-derived biochars from different feedstocks and pyrolysis temperatures. J Anal Appl Pyrolysis 102:137–143. https://doi.org/10.1016/j.jaap.2013.03.004
41. Dehkhoda AM, Gyenge E, Ellis N (2016) A novel method to tailor the porous structure of KOH-activated biochar and its application in capacitive deionization and energy storage. Biomass Bioenergy 87:107–121. https://doi.org/10.1016/j.biombioe.2016.02.023
42. Banik C, Lawrinenko M, Bakshi S, Laird DA (2018) Impact of pyrolysis temperature and feedstock on surface charge and functional group chemistry of biochars. J Environ Qual 47:452–461. https://doi.org/10.2134/jeq2017.11.0432
43. Albanese L, Baronti S, Liguori F et al (2019) Hydrodynamic cavitation as an energy efficient process to increase biochar surface area and porosity: a case study. J Clean Prod 210:159–169. https://doi.org/10.1016/j.jclepro.2018.10.341
44. Mohamed I, Ali M, Ahmed N et al (2018) Cow manure-loaded biochar changes Cd fractionation and phytotoxicity potential for wheat in a natural acidic contaminated soil. Ecotoxicol Environ Saf 162:348–353. https://doi.org/10.1016/j.ecoenv.2018.06.065
45. Kim KH, Kim JY, Cho TS, Choi JW (2012) Influence of pyrolysis temperature on physicochemical properties of biochar obtained from the fast pyrolysis of pitch pine (Pinus rigida). Bioresour Technol 118:158–162. https://doi.org/10.1016/j.biortech.2012.04.094
46. Mimmo T, Panzacchi P, Baratieri M et al (2014) Effect of pyrolysis temperature on miscanthus (Miscanthus × giganteus) biochar physical, chemical and functional properties. Biomass Bioenergy 62:149–157. https://doi.org/10.1016/j.biombioe.2014.01.004
47. Zhang H, Voroney RP, Price GW (2015) Effects of temperature and processing conditions on biochar chemical properties and their influence on soil C and N transformations. Soil Biol Biochem 83:19–28. https://doi.org/10.1016/j.soilbio.2015.01.006
48. Yuan H, Lu T, Wang Y et al (2014) Influence of pyrolysis temperature and holding time on properties of biochar derived from medicinal herb (radix isatidis) residue and its effect on soil CO_2 emission. J Anal Appl Pyrolysis 110:277–284. https://doi.org/10.1016/j.jaap.2014.09.016
49. fei TX, guo LY, ling GY et al (2016) Biochar-based nano-composites for the decontamination of wastewater: a review. Bioresour Technol 212:318–333. https://doi.org/10.1016/j.biortech.2016.04.093
50. Amusat SO, Kebede TG, Dube S, Nindi MM (2021) Ball-milling synthesis of biochar and biochar–based nanocomposites and prospects for removal of emerging contaminants: A review. J Water Process Eng 41:101993. https://doi.org/10.1016/j.jwpe.2021.101993
51. Han H, Rafiq MK, Zhou T et al (2019) A critical review of clay-based composites with enhanced adsorption performance for metal and organic pollutants. J Hazard Mater 369:780–796. https://doi.org/10.1016/j.jhazmat.2019.02.003
52. Zhang M, Gao B, Varnoosfaderani S et al (2013) Preparation and characterization of a novel magnetic biochar for arsenic removal. Bioresour Technol 130:457–462. https://doi.org/10.1016/j.biortech.2012.11.132

53. Inyang M, Gao B, Zimmerman A et al (2014) Synthesis, characterization, and dye sorption ability of carbon nanotube-biochar nanocomposites. Chem Eng J 236:39–46. https://doi.org/10.1016/j.cej.2013.09.074
54. Silvestri S, Stefanello N, Sulkovski AA, Foletto EL (2020) Preparation of TiO_2 supported on MDF biochar for simultaneous removal of methylene blue by adsorption and photocatalysis. J Chem Technol Biotechnol 95:2723–2729. https://doi.org/10.1002/jctb.6279
55. Lyu H, Zhang Q, Shen B (2020) Application of biochar and its composites in catalysis. Chemosphere 240. https://doi.org/10.1016/j.chemosphere.2019.124842
56. Premarathna KSD, Rajapaksha AU, Sarkar B et al (2019) Biochar-based engineered composites for sorptive decontamination of water: a review. Chem Eng J 372:536–550. https://doi.org/10.1016/j.cej.2019.04.097
57. Jamkhande PG, Ghule NW, Bamer AH, Kalaskar MG (2019) Metal nanoparticles synthesis: an overview on methods of preparation, advantages and disadvantages, and applications. J Drug Deliv Sci Technol 53:101174. https://doi.org/10.1016/j.jddst.2019.101174
58. Mukherjee A, Goswami N, Dhak D (2022) Photocatalytic remediation of industrial dye waste streams using biochar and metal-biochar hybrids: a critical review. Chem Africa 6:609–628. https://doi.org/10.1007/s42250-022-00467-5
59. Yu KL, Lee XJ, Ong HC et al (2021) Adsorptive removal of cationic methylene blue and anionic Congo red dyes using wet-torrefied microalgal biochar: equilibrium, kinetic and mechanism modeling. Environ Pollut 272:115986. https://doi.org/10.1016/j.envpol.2020.115986
60. Wu J, Yang J, Feng P et al (2020) High-efficiency removal of dyes from wastewater by fully recycling litchi peel biochar. Chemosphere 246:125734. https://doi.org/10.1016/j.chemosphere.2019.125734
61. Bagheri AR, Aramesh N, Khan AA et al (2021) Molecularly imprinted polymers-based adsorption and photocatalytic approaches for mitigation of environmentally-hazardous pollutants - a review. J Environ Chem Eng 9:104879. https://doi.org/10.1016/j.jece.2020.104879
62. El-Bassi L, Azzaz AA, Jellali S et al (2021) Application of olive mill waste-based biochars in agriculture: Impact on soil properties, enzymatic activities and tomato growth. Sci Total Environ 755:142531. https://doi.org/10.1016/j.scitotenv.2020.142531
63. Li A, Ge W, Liu L, Qiu G (2022) Preparation, adsorption performance and mechanism of MgO-loaded biochar in wastewater treatment: a review. Environ Res 212:113341. https://doi.org/10.1016/j.envres.2022.113341
64. Amdeha E (2023) Smart nanomaterials for photo-catalytic applications. In: Bansal SA, Khanna V, Balakrishnan N, Gupta P (eds) Diversity and Applications of New Age Nanoparticles. IGI Global, pp 112–154 10.4018/978-1-6684-7358-0.ch005
65. Qiu M, Hu B, Chen Z et al (2021) Challenges of organic pollutant photocatalysis by biochar-based catalysts. Biochar 3:117–123. https://doi.org/10.1007/s42773-021-00098-y
66. Hao M, Qiu M, Yang H et al (2021) Recent advances on preparation and environmental applications of MOF-derived carbons in catalysis. Sci Total Environ 760:143333. https://doi.org/10.1016/j.scitotenv.2020.143333
67. Amdeha E, Salem MS (2022) Facile green synthesis of ZnO supported on exfoliated graphite for photocatalytic degradation of dye under UV and visible-light irradiation. Egypt J Chem 65:557–569. https://doi.org/10.21608/EJCHEM.2022.130532.5931
68. Cui J, Zhang F, Li H et al (2020) Recent progress in biochar-based photocatalysts for wastewater treatment: synthesis, mechanisms, and applications. Appl Sci 10. https://doi.org/10.3390/app10031019
69. Sharma S, Dutta V, Raizada P et al (2021) Tailoring cadmium sulfide-based photocatalytic nanomaterials for water decontamination: a review. Environ Chem Lett 19:271–306. https://doi.org/10.1007/s10311-020-01066-x
70. Hasija V, Nguyen VH, Kumar A et al (2021) Advanced activation of persulfate by polymeric g-C_3N_4 based photocatalysts for environmental remediation: A review. J Hazard Mater 413. https://doi.org/10.1016/j.jhazmat.2021.125324
71. El-Salamony RA, Amdeha E, El Shafey AM, Al Sabagh AM (2023) Preparation and characterisation of Ce-doped SiO_2 nanomaterials as effective photo-catalyst under visible light. Int J Environ Anal Chem 103:868–883. https://doi.org/10.1080/03067319.2020.1865328
72. Mostafa EM, Amdeha E (2022) Enhanced photocatalytic degradation of malachite green dye by highly stable visible-light-responsive Fe-based tri-composite photocatalysts. Environ Sci Pollut Res 29:69861–69874. https://doi.org/10.1007/s11356-022-20745-6
73. Bayode AA, Vieira EM, Moodley R et al (2021) Tuning ZnO/GO p-n heterostructure with carbon interlayer supported on clay for visible-light catalysis: Removal of steroid estrogens from water. Chem Eng J 420:127668. https://doi.org/10.1016/j.cej.2020.127668
74. Mashile GP, Selahle SK, Mpupa A et al (2022) Remediation of emerging pollutants through various wastewater treatment processes. Emerg Freshw Pollut:137–150. https://doi.org/10.1016/b978-0-12-822850-0.00005-3
75. Ahamad T, Naushad M, Ubaidullah M, Alshehri S (2020) Fabrication of highly porous polymeric nanocomposite for the removal of radioactive U(VI) and Eu(III) ions from aqueous solution. Polymers (Basel) 12:1–16. https://doi.org/10.3390/polym12122940
76. Vakili M, Deng S, Cagnetta G et al (2019) Regeneration of chitosan-based adsorbents used in heavy metal adsorption: a review. Sep Purif Technol 224:373–387. https://doi.org/10.1016/j.seppur.2019.05.040
77. Gusain R, Gupta K, Joshi P, Khatri OP (2019) Adsorptive removal and photocatalytic degradation of organic pollutants using metal oxides and their composites: a comprehensive review. Adv Colloid Interface Sci 272. https://doi.org/10.1016/j.cis.2019.102009
78. Wei X, Wang X, Pu Y et al (2021) Facile ball-milling synthesis of CeO_2/g-C_3N_4 Z-scheme heterojunction for synergistic adsorption and photodegradation of methylene blue: characteristics, kinetics, models, and mechanisms. Chem Eng J 420:127719. https://doi.org/10.1016/j.cej.2020.127719
79. Adeola AO, Forbes PBC (2021) Advances in water treatment technologies for removal of polycyclic aromatic hydrocarbons: Existing concepts, emerging trends, and future prospects. Water Environ Res 93:343–359. https://doi.org/10.1002/wer.1420
80. Mudhoo A, Sillanpää M (2021) Magnetic nanoadsorbents for micropollutant removal in real water treatment: a review. Environ Chem Lett 19:4393–4413. https://doi.org/10.1007/s10311-021-01289-6
81. Adeola AO, Ore OT, Fapohunda O et al (2022) Psychotropic drugs of emerging concerns in aquatic systems: ecotoxicology and remediation approaches. Chem Africa 5:481–508. https://doi.org/10.1007/s42250-022-00334-3
82. Pathak S, Sakhiya AK, Anand A et al (2022) A state-of-the-art review of various adsorption media employed for the removal of toxic Polycyclic aromatic hydrocarbons (PAHs): an approach towards a cleaner environment. J Water Process Eng 47:102674. https://doi.org/10.1016/j.jwpe.2022.102674

83. Adeola AO, Akingboye AS, Ore OT et al (2022) Crude oil exploration in Africa: socio-economic implications, environmental impacts, and mitigation strategies. Environ Syst Decis 42:26–50. https://doi.org/10.1007/s10669-021-09827-x
84. Niazi NK, Bibi I, Shahid M et al (2018) Arsenic removal by Japanese oak wood biochar in aqueous solutions and well water: investigating arsenic fate using integrated spectroscopic and microscopic techniques. Sci Total Environ 621:1642–1651. https://doi.org/10.1016/j.scitotenv.2017.10.063
85. Niazi NK, Bibi I, Shahid M et al (2018) Arsenic removal by perilla leaf biochar in aqueous solutions and groundwater: an integrated spectroscopic and microscopic examination. Environ Pollut 232:31–41. https://doi.org/10.1016/j.envpol.2017.09.051
86. Ahmed W, Núñez-Delgado A, Mehmood S et al (2021) Highly efficient uranium (VI) capture from aqueous solution by means of a hydroxyapatite-biochar nanocomposite: Adsorption behavior and mechanism. Environ Res 201:111518. https://doi.org/10.1016/j.envres.2021.111518
87. Jung KW, Lee SY, Choi JW, Lee YJ (2019) A facile one-pot hydrothermal synthesis of hydroxyapatite/biochar nanocomposites: adsorption behavior and mechanisms for the removal of copper(II) from aqueous media. Chem Eng J 369:529–541. https://doi.org/10.1016/j.cej.2019.03.102
88. Yi Y, Huang Z, Lu B et al (2020) Magnetic biochar for environmental remediation: a review. Bioresour Technol 298:122468. https://doi.org/10.1016/j.biortech.2019.122468
89. Tan Z, Wang Y, Kasiulienė A et al (2017) Cadmium removal potential by rice straw-derived magnetic biochar. Clean Technol Environ Policy 19:761–774. https://doi.org/10.1007/s10098-016-1264-2
90. Shen Y, Ma D, Ge X (2017) CO_2-looping in biomass pyrolysis or gasification. Sustain Energy Fuels 1:1700–1729. https://doi.org/10.1039/c7se00279c
91. Bai L, Huang A, Feng J et al (2022) One-step microwave pyrolysis synthesis of bagasse biochar/ ferrites nanocomposite and synergistic effect on As(V) adsorption in water. Mater Chem Phys 283:126035. https://doi.org/10.1016/j.matchemphys.2022.126035
92. Yao X, Ji L, Guo J et al (2020) Magnetic activated biochar nanocomposites derived from wakame and its application in methylene blue adsorption. Bioresour Technol 302:122842. https://doi.org/10.1016/j.biortech.2020.122842
93. Kumar Prajapati A, Kumar Mondal M (2022) Green synthesis of Fe_3O_4-onion peel biochar nanocomposites for adsorption of Cr(VI), methylene blue and congo red dye from aqueous solutions. J Mol Liq 349:118161. https://doi.org/10.1016/j.molliq.2021.118161
94. Batool S, Shah AA, Abu Bakar AF et al (2022) Removal of organochlorine pesticides using zerovalent iron supported on biochar nanocomposite from Nephelium lappaceum (Rambutan) fruit peel waste. Chemosphere 289:133011. https://doi.org/10.1016/j.chemosphere.2021.133011
95. Shaikh WA, Islam RU, Chakraborty S (2021) Stable silver nanoparticle doped mesoporous biochar-based nanocomposite for efficient removal of toxic dyes. J Environ Chem Eng 9:104982. https://doi.org/10.1016/j.jece.2020.104982
96. Liu Y, Cao S, Xi C et al (2021) A new nanocomposite assembled with metal organic framework and magnetic biochar derived from pomelo peels: a highly efficient adsorbent for ketamine in wastewater. J Environ Chem Eng 9:106207. https://doi.org/10.1016/j.jece.2021.106207
97. Mukherjee A, Kundu S, Chatterjee D, Dhak D (2022) A critical review on photoreduction using metal–organic frameworks: kinetics, pH and mechanistic studies and anthropogenic/natural sources of Cr(VI). Chem Africa 5:1783–1796. https://doi.org/10.1007/s42250-021-00295-z
98. Yu F, Tian F, Zou H et al (2021) ZnO/biochar nanocomposites via solvent free ball milling for enhanced adsorption and photocatalytic degradation of methylene blue. J Hazard Mater 415:125511. https://doi.org/10.1016/j.jhazmat.2021.125511
99. Kamal A, Saleem MH, Alshaya H et al (2022) Ball-milled synthesis of maize biochar-ZnO nanocomposite (MB-ZnO) and estimation of its photocatalytic ability against different organic and inorganic pollutants. J Saudi Chem Soc 26:101445. https://doi.org/10.1016/j.jscs.2022.101445
100. Wang T, Zheng J, Cai J et al (2022) Visible-light-driven photocatalytic degradation of dye and antibiotics by activated biochar composited with K^+ doped g-C_3N_4: Effects, mechanisms, actual wastewater treatment and disinfection. Sci Total Environ 839:155955. https://doi.org/10.1016/j.scitotenv.2022.155955
101. Fatimah I, Purwiandono G, Sahroni I et al (2022) Magnetically-separable photocatalyst of magnetic biochar from snake fruit peel for rhodamine B photooxidation. Environ Nanotechnology, Monit Manag 17:100669. https://doi.org/10.1016/j.enmm.2022.100669
102. Cheng L, Zhang Y, Fan W, Ji Y (2022) Synergistic adsorption-photocatalysis for dyes removal by a novel biochar–based Z-scheme heterojunction BC/2ZIS/WO_3: Mechanistic investigation and degradation pathways. Chem Eng J 445:136677. https://doi.org/10.1016/j.cej.2022.136677
103. Kang F, Shi C, Li W et al (2022) Honeycomb like CdS/sulphur-modified biochar composites with enhanced adsorption-photocatalytic capacity for effective removal of rhodamine B. J Environ Chem Eng 10:106942. https://doi.org/10.1016/j.jece.2021.106942
104. Siara S, Elvis C, Harishkumar R, Velayudhaperumal Chellam P (2022) $ZnAl_2O_4$ supported on lychee-biochar applied to ibuprofen photodegradation. Mater Res Bull 145:111530. https://doi.org/10.1016/j.materresbull.2021.111530
105. Shaikh WA, Kumar A, Chakraborty S et al (2022) Biochar-based nanocomposite from waste tea leaf for toxic dye removal: From facile fabrication to functional fitness. Chemosphere 291:132788. https://doi.org/10.1016/j.chemosphere.2021.132788
106. Shaikh WA, Chakraborty S, Islam RU (2020) Photocatalytic degradation of rhodamine B under UV irradiation using Shorea robusta leaf extract-mediated bio-synthesized silver nanoparticles. Int J Environ Sci Technol 17:2059–2072. https://doi.org/10.1007/s13762-019-02473-6
107. Shaikh WA, Alam MA, Alam MO et al (2020) Enhanced aqueous phase arsenic removal by a biochar based iron nanocomposite. Environ Technol Innov 19:100936. https://doi.org/10.1016/j.eti.2020.100936
108. Azari A, Nabizadeh R, Nasseri S et al (2020) Comprehensive systematic review and meta-analysis of dyes adsorption by carbon-based adsorbent materials: classification and analysis of last decade studies. Chemosphere 250:126238. https://doi.org/10.1016/j.chemosphere.2020.126238
109. Zare EN, Iftekhar S, Park Y et al (2021) An overview on non-spherical semiconductors for heterogeneous photocatalytic degradation of organic water contaminants. Chemosphere 280:130907. https://doi.org/10.1016/j.chemosphere.2021.130907
110. Ammar SH, Ibrahim Elaibi A, Sh. Mohammed I (2020) Core/shell Fe_3O_4@Al_2O_3-PMo magnetic nanocatalyst for photocatalytic degradation of organic pollutants in an internal loop airlift reactor. J Water Process Eng 37:101240. https://doi.org/10.1016/j.jwpe.2020.101240
111. Sun J, Qiao L, Sun S, Wang G (2008) Photocatalytic degradation of Orange G on nitrogen-doped TiO_2 catalysts under visible light and sunlight irradiation. J Hazard Mater 155:312–319. https://doi.org/10.1016/j.jhazmat.2007.11.062
112. Riga A, Soutsas K, Ntampegliotis K et al (2007) Effect of system parameters and of inorganic salts on the decolorization and degradation of Procion H-exl dyes. Comparison of H_2O_2/UV, Fenton, UV/Fenton, TiO_2/UV and TiO_2/UV/H_2O_2 processes. Desalination 211:72–86. https://doi.org/10.1016/j.desal.2006.04.082

113. Shafi RF, Ammar SH, Rashed MK (2021) Catalytic/photocatalytic oxidative desulfurization activities of heteropolyacid immobilized on magnetic polythiophene nanocatalyst. J Sulfur Chem 42:443–463. https://doi.org/10.1080/17415993.2021.1906245
114. Jabbar ZH, Ebrahim SE (2021) Highly efficient visible-light-driven photocatalytic degradation of organic pollutants by using magnetically separable supported heterogeneous nanocomposites ($SiO_2/Fe_3O_4/Ag_2WO_4$). Environ Nanotechnology, Monit Manag 16:100554. https://doi.org/10.1016/j.enmm.2021.100554
115. Nadeem N, Zahid M, Rehan ZA et al (2022) Improved photocatalytic degradation of dye using coal fly ash-based zinc ferrite ($CFA/ZnFe_2O_4$) composite. Int J Environ Sci Technol 19:3045–3060. https://doi.org/10.1007/s13762-021-03255-9
116. Zhang J, Li X, Zhang X et al (2018) Geochemical and geological characterization of marine–continental transitional shales from Longtan Formation in Yangtze area, South China. Mar Pet Geol 96:1–15. https://doi.org/10.1016/j.marpetgeo.2018.05.020
117. Liu B, Qiao M, Wang Y et al (2017) Persulfate enhanced photocatalytic degradation of bisphenol A by g-C_3N_4 nanosheets under visible light irradiation. Chemosphere 189:115–122. https://doi.org/10.1016/j.chemosphere.2017.08.169
118. Zheng Y, Cao L, Xing G et al (2019) Microscale flower-like magnesium oxide for highly efficient photocatalytic degradation of organic dyes in aqueous solution. RSC Adv 9:7338–7348. https://doi.org/10.1039/C8RA10385B
119. Chu L, Zhang J, Wu Z et al (2020) Solar-driven photocatalytic removal of organic pollutants over direct Z-scheme coral-branch shape Bi_2O_3/SnO_2 composites. Mater Charact 159:110036. https://doi.org/10.1016/j.matchar.2019.110036
120. Ma Y, Li M, Li P et al (2021) Hydrothermal synthesis of magnetic sludge biochar for tetracycline and ciprofloxacin adsorptive removal. Bioresour Technol 319:124199. https://doi.org/10.1016/j.biortech.2020.124199
121. Qu J, Shi J, Wang Y et al (2022) Applications of functionalized magnetic biochar in environmental remediation: a review. J Hazard Mater 434:128841. https://doi.org/10.1016/j.jhazmat.2022.128841
122. He C, Xia W, Zhou C et al (2022) Rational design to manganese and oxygen co-doped polymeric carbon nitride for efficient nonradical activation of peroxymonosulfate and the mechanism insight. Chem Eng J 430:132751. https://doi.org/10.1016/j.cej.2021.132751
123. Yuan X, Qin W, Lei X et al (2018) Efficient enhancement of ozonation performance via ZVZ immobilized g-C_3N_4 towards superior oxidation of micropollutants. Chemosphere 205:369–379. https://doi.org/10.1016/j.chemosphere.2018.04.121
124. Li Y, Li J, Pan Y et al (2020) Peroxymonosulfate activation on $FeCo_2S_4$ modified g-C_3N_4 ($FeCo_2S_4$-CN): mechanism of singlet oxygen evolution for nonradical efficient degradation of sulfamethoxazole. Chem Eng J 384:123361. https://doi.org/10.1016/j.cej.2019.123361
125. Xu A, Yu D, Qiu Y et al (2022) A novel process of salt tolerance partial denitrification and anammox (ST-PDA) for treating saline wastewater. Bioresour Technol 345:126472. https://doi.org/10.1016/j.biortech.2021.126472
126. Sun X, Yang L, Xing H et al (2013) Synthesis of polyethylenimine-functionalized poly(glycidyl methacrylate) magnetic microspheres and their excellent Cr(VI) ion removal properties. Chem Eng J 234:338–345. https://doi.org/10.1016/j.cej.2013.08.082
127. Qu J, Akindolie MS, Feng Y et al (2020) One-pot hydrothermal synthesis of $NaLa(CO_3)_2$ decorated magnetic biochar for efficient phosphate removal from water: kinetics, isotherms, thermodynamics, mechanisms and reusability exploration. Chem Eng J 394:124915. https://doi.org/10.1016/j.cej.2020.124915
128. Mu Y, Ma H (2021) NaOH-modified mesoporous biochar derived from tea residue for methylene Blue and Orange II removal. Chem Eng Res Des 167:129–140. https://doi.org/10.1016/j.cherd.2021.01.008
129. Sayin F, Akar ST, Akar T (2021) From green biowaste to water treatment applications: utilization of modified new biochar for the efficient removal of ciprofloxacin. Sustain Chem Pharm 24:100522. https://doi.org/10.1016/j.scp.2021.100522
130. Nguyen DLT, Binh QA, Nguyen XC et al (2021) Metal salt-modified biochars derived from agro-waste for effective congo red dye removal. Environ Res 200:111492. https://doi.org/10.1016/j.envres.2021.111492
131. Karimi L, Yazdanshenas ME, Khajavi R et al (2015) Optimizing the photocatalytic properties and the synergistic effects of graphene and nano titanium dioxide immobilized on cotton fabric. Appl Surf Sci 332:665–673. https://doi.org/10.1016/j.apsusc.2015.01.184
132. Jabbar ZH, Ebrahim SE, Ammar SH (2022) Supported heterogeneous nanocomposites ($SiO_2/Fe_3O_4/Ag_2WO_4$) for visible-light-driven photocatalytic disinfection against E. coli. Mater Sci Semicond Process 141:106427. https://doi.org/10.1016/j.mssp.2021.106427
133. Zhang H, Wang Z, Li R et al (2017) TiO_2 supported on reed straw biochar as an adsorptive and photocatalytic composite for the efficient degradation of sulfamethoxazole in aqueous matrices. Chemosphere 185:351–360. https://doi.org/10.1016/j.chemosphere.2017.07.025